Monthly Notices
of the
ROYAL ASTRONOMICAL SOCIETY

MNRAS **469,** 3489–3504 (2017)
Advance Access publication 2017 May 6

doi:10.1093/mnras/stx1081

# Galaxy And Mass Assembly: search for a population of high-entropy galaxy groups

R. J. Pearson,[1⋆] T. J. Ponman,[1⋆] P. Norberg,[2] A. S. G. Robotham,[3] A. Babul,[4] R. G. Bower,[2] I. G. McCarthy,[5] S. Brough,[6] S. P. Driver[3,7] and K. Pimbblet[8,9]

[1]*School of Physics and Astronomy, University of Birmingham, Edgbaston, Birmingham B15 2TT, UK*
[2]*ICC and CEA, Department of Physics, Durham University, South Road, Durham DH1 3LE, UK*
[3]*International Centre for Radio Astronomy Research, University of Western Australia, 35 Stirling Highway, Crawley, WA 6009, Australia*
[4]*Department of Physics and Astronomy, University of Victoria, BC V8X 4M6, Canada*
[5]*Astrophysics Research Institute, Liverpool John Moores University, 146 Brownlow Hill, Liverpool L3 5RF, UK*
[6]*Australian Astronomical Observatory, PO Box 915, North Ryde, NSW 1670, Australia*
[7]*School of Physics and Astronomy, University of St Andrews, North Haugh, St Andrews KY16 9SS, UK*
[8]*E. A. Milne Centre for Astrophysics, University of Hull, Cottingham Road, Kingston-upon-Hull HU6 7RX, UK*
[9]*School of Physics and Astronomy, Monash University, Clayton, VIC 3800, Australia*

Accepted 2017 May 3. Received 2017 May 1; in original form 2016 December 3

## ABSTRACT

Observations with the *Chandra X-ray Observatory* are used to examine the hot gas properties within a sample of 10 galaxy groups selected from the Galaxy And Mass Assembly survey's optical Friends-of-Friends group catalogue. Our groups have been screened to eliminate spurious and unrelaxed systems, and the effectiveness of this procedure is demonstrated by the detection of intergalactic hot gas in 80 per cent of our sample. However, we find that 9 of the 10 are X-ray underluminous by a mean factor of ∼4 compared to typical X-ray-selected samples. Consistent with this, the majority of our groups have gas fractions that are lower and gas entropies somewhat higher than those seen in typical X-ray-selected samples. Two groups, which have high $2\sigma$ lower limits on their gas entropy, are candidates for the population of high-entropy groups predicted by some active galactic nucleus feedback models.

**Key words:** galaxies: clusters: intracluster medium – galaxies: groups: general – X-rays: galaxies: clusters.

## 1 INTRODUCTION

Studies of the hot gas in groups and clusters of galaxies have demonstrated that this gas exhibits entropies in excess of self-similar expectations (e.g. Ponman, Cannon & Navarro 1999; Lloyd-Davies, Ponman & Cannon 2000). Determining how, why and when this entropy was raised is essential to better understand the formation and evolution of both galaxies and galaxy clusters. For example, the processes responsible for raising the gas entropy may be the same as those that maintain the hot gas content of the Universe by preventing runaway cooling of gas into stars (the cooling catastrophe; Balogh et al. 2001).

Early models suggested that entropy had been injected into the intracluster medium (ICM) prior to the full collapse of the cluster (Kaiser 1991; Evrard & Henry 1991). Proposed sources of entropy included supernova feedback and active galactic nuclei (AGNs; Lloyd-Davies et al. 2000; Wu, Fabian & Nulsen 2000; Tozzi & Norman 2001; Babul et al. 2002). Due to the smaller potential wells of groups compared to massive clusters, the entropy injected into gas at group scales can be significant compared to the entropy accrued during halo assembly. Alternatives, such as the action of cooling flows, which preferentially cool low-entropy gas into stars, raising the *mean* ICM entropy (see, e.g. Bryan 2000; Voit & Bryan 2001), have also been proposed. It is now widely recognized that feedback from AGNs reduces the cooling rate within cluster cores, preventing massive cooling flows. Such feedback after cluster collapse provides another potential mechanism for raising the entropy of the ICM (Voit 2005).

Both analytical models (McCarthy et al. 2004, 2008) and hydrodynamical simulations (Lewis et al. 2000; Davé, Oppenheimer & Sivanandam 2008; Schaye et al. 2010; Liang et al. 2016) have been used to explore the evolution of gas within group and cluster haloes, examining the effect of various proposed feedback models. A comparison between the simulations from the Overwhelmingly Large Simulations Project (OWLS; Schaye et al. 2010) and a variety of observational properties of groups (McCarthy et al. 2010, 2011) suggest that the observed raised entropies result from heating of gas by AGN feedback acting within precursor haloes. These models predict a distribution of central entropies broader than

⋆ Email: richard@star.sr.bham.ac.uk (RJP); tjp@star.sr.bham.ac.uk (TJP)

observed in the well-studied X-ray-selected samples of groups, and in particular the existence of a population of systems with very high central entropy. Such high-entropy groups would have low central gas densities, and hence low-surface-brightness X-ray emission. As a result, systems of this sort would be heavily selected against in X-ray-bright samples. The primary aim of this study is to search for a population of galaxy groups ($M \lesssim 10^{14}\,\mathrm{M}_{\odot}$) containing such high-entropy gas.

The starting point for such a search has to be a group sample that has been constructed without any reference to X-ray properties. We therefore start from an optically selected sample of groups. Due to the depth and completeness of the Galaxy and Mass Assembly (GAMA; Driver et al. 2011; Liske et al. 2015) project's spectroscopic survey, we draw our group candidates from their Friends-of-Friends (FoF) group catalogue (Robotham et al. 2011). The difficulty with such optically selected groups is to avoid the contamination of the sample by chance galaxy alignments or by haloes that are yet to fully collapse. Such systems would have little or no diffuse X-ray emissions, and so could be mistaken for high-entropy groups. We therefore apply a number of tests designed to eliminate such spurious or unrelaxed systems from our sample.

The outline of this paper is as follows: In Section 2, we discuss how we select our sample of relaxed optical groups by testing for substructure in the distribution of member galaxies. Section 3 describes the X-ray analysis performed on the *Chandra* data, and Section 4 presents the results for the X-ray luminosity ($L_{\mathrm{X}}$), and the mass and central entropy of the hot gas within our groups. We conclude, in Sections 5 and 6, by discussing the virialization of these groups and the limitations in our analysis that could affect our entropy constraints. Throughout this paper, we adopt a simple $\Lambda$ cold dark matter cosmology with $\Omega_{\mathrm{m}} = 0.3$, $\Omega_{\Lambda} = 0.7$ and $H_0 = 70\,\mathrm{km\,s^{-1}\,Mpc^{-1}}$, with $h = H_0/100\,\mathrm{km\,s^{-1}\,Mpc^{-1}} = 0.7$.

## 2 THE OPTICAL GROUP SAMPLE

To investigate whether a population of high-entropy groups exists, we need to start from a sample of relaxed, optically selected groups. As discussed above, this removes ambiguity in the nature of any observed low $L_{\mathrm{X}}$ groups. The GAMA survey provides an excellent platform from which to begin a study of this nature.

The GAMA project is a broad multiwavelength survey covering $\sim$290 deg$^2$ of the sky. The main optical component of the project is a medium-deep redshift survey conducted with the AAOmega multi-object spectrograph at the Anglo-Australian Observatory. This provides spectra and redshifts (Hopkins et al. 2013) for more than 300 000 galaxies within five sky regions. A grouping analysis has been performed on the galaxies from the first three regions surveyed by Robotham et al. (2011) using an FoF algorithm optimized on a sample of nine realistic mock light cones (Merson et al. 2013). These light cones were generated using the dark matter Millennium Simulation (Springel et al. 2005) populated with galaxies using the Bower et al. (2006) semi-analytic models of galaxy formation, with modifications to reproduce the observed $r$-band, redshift-dependent, GAMA luminosity function of Loveday et al. (2012).

At the time this study began, most of the GAMA survey had been completed to an $r$-band magnitude of only $m_r = 19.4$ mag, and the G3Cv04 group catalogue had been constructed from these data by Robotham et al. (2011). Since then, additional galaxy spectra have been taken, extending the completeness to $m_r = 19.8$ mag and an updated (G3Cv06) group catalogue has been compiled. Our selection of a relaxed group sample, as described in Section 2, makes use of the G3Cv04 group catalogue, and *Chandra* data were acquired for the resulting sample. All subsequent analysis presented here beyond the initial selection makes use of the deeper data available from the G3Cv06 group catalogue.

The G3Cv04 catalogue contained 12 200 FoF groups and clusters with two or more members brighter than $m_r = 19.4$ mag. We first cut the catalogue to restrict it to groups with $N \geq 12$ galaxies for two reasons: First, this essentially eliminates the possibility of spurious groups generated from chance alignment of physically unrelated galaxies, and, secondly, it ensures that we have reasonable galaxy statistics for the substructure analysis we subsequently applied to filter out unrelaxed systems. This initial cut left a catalogue of 205 galaxy groups and clusters. We then restricted the sample to redshifts $z \leq 0.12$, since more distant systems passing our membership criterion are fairly rich clusters, whilst our focus in this study is on galaxy groups ($M_{500} \lesssim 10^{14}\,\mathrm{M}_{\odot}$). This redshift cut reduced the sample to 64 galaxy groups that were subjected to the substructure screening described below. We found that these limits on richness and redshift provided the best compromise between the conflicting requirements of increasing the number of candidate groups to select from whilst ensuring statistically useful numbers of group members and reducing the likelihood of including clusters.

### 2.1 Selection

In order to be confident that low X-ray luminosity in any of our groups is indicative of high-entropy gas, it is important to restrict our sample to systems that are collapsed and dynamically relaxed. To do this, we applied a number of tests to assess their degree of substructure. A highly substructured group is likely to be collapsing for the first time, or to have suffered a recent major merger.

Another advantage of relaxed systems is that their masses can be more reliably estimated, and should be closely related to their X-ray properties. Since we use optical mass estimates to predict the X-ray properties of our groups, reliable mass estimates are important for correctly judging the exposure times required to acquire X-ray data of sufficient depth for our study. It is especially important to avoid selecting groups whose masses are overestimated, which would result in predicted exposure times that would be too short.

The substructure statistics employed were calibrated on mock G3Cv04 data constructed for the GAMA project. Using the mock haloes and with known masses and masses predicted from their optical luminosities (see Section 2.4), we tune the selection to discriminate against groups whose mass estimates are more than a factor of 2 larger than the true halo mass.

The selection and calibration of the algorithms we used proceeded as follows. First, we identified a set of substructure statistics that had useful discriminating power to select mock groups with 'good' predicted masses. Secondly, we established a set of thresholds for the adopted statistics that, in combination, maximized the number of mock groups recovered with satisfactory mass estimates. Due to the importance of rejecting groups with overestimated masses, we insisted that our screening process should essentially eliminate any systems whose masses were overestimated by more than a factor of 2. Finally, having tuned our selection criteria on mock groups, we applied this filter to the real G3Cv04 sample.

### 2.2 Substructure statistics

We initially examined nine different substructure statistics that probed the spatial and velocity distributions of the galaxies within a group. Six of these were drawn from the compilation of Pinkney et al. (1996). Two more (an axial ratio and a group symmetry test)

were based upon the output of the Robotham et al. (2011) group analysis, with a further statistic used specifically to examine the distribution of galaxy velocities. It was found that a combination of three of these tests was able to effectively discriminate between systems for which the GAMA mass estimates described in Section 2.4 were reliable, and those for which they were not. Adding further substructure tests to this set produced negligible further gains. Our chosen set of substructure tests consisted of two spatial symmetry statistics: the $\beta_{\rm sym}$-test and the angular separation test (Pinkney et al. 1996), together with the Anderson–Darling test for normality (Thode 2002) in the velocity histogram, implemented through the NORTEST package (Gross & Ligges 2012, and references therein) for the R statistical package (R Development Core Team 2009). Two of these tests, the $\beta_{\rm sym}$-test and the angular separation test, require an optical group centre. A centroid was calculated in each case by taking an unweighted centroid of group galaxies within a radius that was iteratively shrunk until it encompassed 50 per cent of a given group's galaxies.

#### 2.2.1 *The $\beta_{\rm sym}$-test*

This substructure test, discussed in West, Oemler & Dekel (1988) and Pinkney et al. (1996), looks for deviations from mirror symmetry caused by substructure within a group halo. The test proceeds by taking each galaxy and estimating the mean separation, $d_i$, of the $\sqrt{N}$ nearest galaxies to it, where $N$ is the total number of galaxies within the cluster. This distance is then compared to the same quantity calculated about a point diametrically opposite to the galaxy, $d_{\rm o}$, through a central point.

For the $i$th galaxy, $\beta_{\rm sym}$ is then defined as

$$\beta_{{\rm sym},i} = \log\left(\frac{d_{\rm o}}{d_i}\right). \quad (1)$$

The mean value of $\beta_{\rm sym}$ for all galaxies is the unnormalized $\beta_{\rm sym}$-statistic. For an unsubstructured, symmetric system, $\beta_{\rm sym} \approx 0$.

#### 2.2.2 *The angular separation test*

The angular separation test (hereafter AST; West et al. 1988; Pinkney et al. 1996), examines the projected angular distribution of galaxies within the cluster, testing for an excess of small angular separations that could indicate substructure. The AST first determines the mean harmonic separation of members

$$\theta_{\rm hm} = \left[\frac{2}{N(N-1)}\sum_{i=1;i>j}^{N}\theta_{ij}^{-1}\right]^{-1}, \quad (2)$$

where $N$ is again the number of galaxies in the group or cluster and $\theta_{ij}$ is the angular separation of two galaxies relative to the centre of the group. Substructures such as infalling groups should therefore reduce the value of $\theta_{\rm hm}$ relative to a similar halo without any substructure.

The values for both the $\beta_{\rm sym}$-test and for AST are finally normalized by their values from the 'null hypothesis' – a value of the statistic when no substructure is present. This accounts for any contributions to the measured statistic from statistical noise in the population. To generate the null hypothesis, we perform the tests on 1000 realizations of the cluster data where the azimuthal positions of the galaxies have been randomized. We then take the mean of these ensembles to represent the substructure-less null hypothesis. The final test statistics, $\zeta_\beta$ and $\zeta_{\rm AST}$, are

$$\zeta_\beta = \beta_{\rm sym}/\beta_{\rm sym,null} \quad \text{and} \quad \zeta_{\rm AST} = \theta_{\rm null}/\theta_{\rm hm}. \quad (3)$$

With this normalization, substructure-less groups have statistic values of $\approx$1, whilst substructured systems will have statistics $>$1. The significance of the statistic can be easily quantified since it is the fraction of the 1000 randomizations that have *more* substructure than the measured statistic.

#### 2.2.3 *Anderson–Darling test*

Within a virialized structure, we expect the velocity of galaxies to be distributed as a Gaussian along the line of sight. Recent cluster merger activity or incomplete virialization, as well as inclusion of physically unconnected galaxies in a group, would be expected to cause deviations from this distribution, for example, through introducing bimodality or asymmetries in the velocity histogram. The Anderson–Darling test (hereafter the AD test; Thode 2002) examines whether a sample is consistent with having been drawn from a normal distribution, and can therefore be useful for testing for such deviations. As a reasonable proxy for galaxy velocities, we apply the test to the redshifts of member galaxies.

Here we describe the AD test as laid out by Thode (2002) and as implemented by the NORTEST package (Gross & Ligges 2012). The AD test proceeds by first taking the data, in this case, galaxy redshifts, $z$, and sorting and scaling them relative to the mean, $\bar{z}$, and standard deviation, $\sigma_z$, of the sample:

$$z' = \frac{z - \bar{z}}{\sigma_z}. \quad (4)$$

The statistic, $A^2$, is then determined using the normal cumulative distribution function $\Phi$ as

$$A^2 = -N - \frac{1}{N}\sum_{i}^{N}[2i-1][\ln(\Phi(z'_i)) + \ln(1-\Phi(z'_{N-i+1}))], \quad (5)$$

where $N$ is the sample size. The significance of $A^2$, $p(A^2)$, can then be found as per table 4.9 of D'Agostino & Stephens (1986), where a modified statistic, $A^{2\star}$, is adopted such that

$$A^{2\star} = \left(1 + \frac{0.75}{N} + \frac{2.25}{N^2}\right)A^2. \quad (6)$$

We use $p(A^2)$ as our substructure indicator. To be consistent with the sense of $\zeta_\beta$ and $\zeta_{\rm AST}$, we define $\zeta_{\rm AD} = 1/p(A^2)$ such that a value $\approx$1 indicates low levels of substructure, and $\zeta_{\rm AD} \gg 1$ shows substantial non-Gaussian structure in the velocity histogram.

### 2.3 Calibration

Using the mock galaxy groups, we calibrated a set of threshold values for our three substructure statistics that selected out groups meeting the criteria discussed in Section 2.1 for reliability of mass estimation. To ensure joint optimization of the three substructure statistics, we explored a gridded ($\zeta_\beta$, $\zeta_{\rm AST}$, $\zeta_{\rm AD}$) parameter space, characterizing each combination by the accuracy of the predicted masses (see Section 2.4) for the groups that passed the filter. Using one of the GAMA mock volumes, we optimized the threshold values to discard all groups with predicted masses greater than twice the true halo mass whilst maximizing the number of groups with mass estimates within a factor of 2 of the true mass. As each mock FoF group may link galaxies from multiple dark matter haloes, we take the true mass FoF group to be the mass of the halo that contributes the most galaxies to the group.

The resulting calibration accepted groups with substructure measures $\zeta_\beta < 1.9$, $\zeta_{\rm AST} < 1.68$ and $\zeta_{\rm AD} < 1.82$. Of the 62 groups

**Table 1.** Summary of the predicted properties of our selected groups based on the G3Cv06 group catalogue and associated X-ray observations.

| Group ID[a] | Central[b] galaxy | $\alpha^c$ | $\delta^c$ | $z^c$ | $N_{\rm fof}{}^d$ | $M_{500,\,\rm Pred}{}^e$ ($10^{13}\,h_{70}^{-1}\,{\rm M}_\odot$) | $r_{500,\,\rm Pred}{}^e$ ($h_{70}^{-1}$ kpc) | $T_{500,\,\rm Pred}{}^f$ (keV) | $t_{\rm exp}{}^g$ (ks) | ObsID[g] |
|---|---|---|---|---|---|---|---|---|---|---|
| 100053 (100072) | 279874 | 139.74 | 1.149 | 0.0874 | 32 (23) | 5.9 | 576 | 1.5 | 9.9 | 14001 |
| 200015 (200011) | 30699 | 176.53 | −1.094 | 0.1175 | 34 (33) | 4.8 | 532 | 1.4 | 15.8 | 14002 |
| 200017 (200014) | 536417 | 182.26 | −0.965 | 0.1132 | 22 (20) | 4.0 | 502 | 1.2 | 34.3 | 14005 |
| 200043 (200018) | 537303 | 184.71 | −1.047 | 0.1195 | 23 (22) | 5.2 | 548 | 1.4 | 10.6 | 14003 |
| 200054 (200036) | 136792 | 176.10 | −1.851 | 0.1069 | 23 (17) | 4.6 | 527 | 1.3 | 24.7 | 14004 |
| 200099 (200034) | 534758 | 174.93 | −1.030 | 0.0777 | 23 (24) | 4.7 | 536 | 1.3 | 14.9 | 14000 |
| 200115 (200063) | 136847 | 176.28 | −1.758 | 0.0276 | 18 (17) | 2.6 | 448 | 0.94 | 24.7 | 14007 |
| 200130 (200003) | 230776 | 181.11 | 1.896 | 0.0200 | 35 (46) | 7.2 | 629 | 1.7 | 30.0 | 3234 |
| 300008 (300006) | 15899 | 217.19 | 0.708 | 0.1027 | 23 (20) | 3.6 | 489 | 1.1 | 52.6 | 14006 |
| 300067 (300028) | 594961 | 222.75 | −0.036 | 0.0429 | 22 (24) | 2.6 | 446 | 0.94 | 25.7 | 14008 |

[a]Group ID in parentheses shows the G3Cv04 group ID. Group IDs of the form 1*xxxxx*, 2*xxxxx* and 3*xxxxx* indicate groups from GAMA regions G09, G12 and G15, respectively.
[b]G3Cv06 galaxy ID for galaxies identified as optical central galaxies using our iterative centroid algorithm described in Section 2.5.
[c]Listed centres correspond to the galaxy associated with the X-ray peaks. In cases where no emission is detected, we assign a central galaxy as described in Section 2.5. For group 200115, where the X-ray centroid is offset from the brightest group galaxies, we use the X-ray centroid. Redshifts are as defined by the Robotham et al. (2011) FoF group finder.
[d]Group FoF multiplicities from the G3Cv06 group catalogue (corresponding values from the G3Cv04 catalogue are given in parentheses).
[e]$r$-band luminosity derived mass estimates as described in the main text. Predicted $r_{500}$ assumes the critical density of the Universe at redshift $z$ (Section 2.4).
[f]Temperatures estimated using the $M$–$T$ relation of Sun et al. (2009).
[g]Exposure time and *Chandra* observation ID of each observation used. With the exception of the archival data for 200130, this was calculated using group properties from the G3Cv04 group catalogue.

with $N_{\rm FoF} \geq 12$ and $z \leq 0.12$ within the mock volume used for the calibration, these thresholds were able to exclude all groups whose masses were overestimated by a factor of 2 whilst allowing 17 per cent of the 42 groups with masses within a factor of 2 (i.e. 'accurate' mass estimates) to pass. Using the same set of thresholds on the other eight mock volumes, which contained 763 groups in total, we found that the filter allowed 16 per cent of groups with 'accurate' masses to pass whilst allowing only 6 per cent contamination by groups whose masses are overpredicted by a factor of $\geq$2. Note that our filter will allow through some groups whose masses are significantly *underestimated*.

### 2.4 Group sample

Applying the calibrated substructure filters to the observed G3Cv04 group catalogue resulted in a sample of 18 groups with $N_{\rm FoF} \geq 12$ and $z \leq 0.12$. Our aim was then to obtain, for as many of these as possible, *Chandra* X-ray observations of a depth sufficient to detect the intragroup gas, even if it has entropy higher than that normally expected within a collapsed group. In order to calculate the required X-ray exposure times, we needed estimates of the luminosity and temperature of the hot intragroup gas for each target. For typical groups, both properties are found to correlate strongly with group mass (e.g. Sun et al. 2009), so we use estimated group halo mass as the basis for our prediction. Group mass has been found to correlate well with optical luminosity (e.g. Popesso et al. 2007), so we adopted the group $r$-band luminosity as a predictor for group mass, using this, in turn, to predict the X-ray properties. We use the relation

$$\frac{M_{\rm GAMA,DHalo}}{h^{-1}\,{\rm M}_\odot} = 10^{1.37}\left(\frac{L_r}{h^{-2}\,{\rm L}_\odot}\right)^{1.09}, \quad (7)$$

where $L_r$ is the total $r$-band luminosity of the FoF group. This is estimated from the observed $r$-band luminosity of the FoF-linked galaxies ($L_{\rm obs}$) using $L_r = BL_{\rm obs}f(z)$, where $f(z)$ is an extrapolation factor to account for GAMA's flux limit and $B = 1.04$ is a correction factor dependent on both group richness and redshift calibrated on the GAMA mock catalogues (Robotham et al. 2011). This quantity is available directly from the group catalogue. We compare this relation to recent relations obtained by Han et al. (2015) and Viola et al. (2015), who both determined mass-observable relations for GAMA groups using weak lensing. They find $M_{\rm halo} \propto L_r^{1.08\pm0.22}$ and $M_{200} \propto L_r^{1.16\pm0.13}$, respectively, comparable to that used here.

Equation (7) was calibrated using mock groups with dark halo masses $M_{\rm DHalo}$ (Jiang et al. 2014; Tankard-Evans 2015). These luminosity-derived masses $M_{\rm GAMA,\,DHalo}$ were then converted into overdensity masses, $M_{500}$ (mass within the region where mean density is 500 times the critical density of the Universe), using $M_{500} = 10^{0.34}M_{\rm GAMA,DHalo}^{0.96}$, estimated from simulated dark matter distributions (Jiang et al. 2014; Tankard-Evans 2015).

The resulting values of $M_{500}$ were then used to predict $r_{500}$ radii, assuming a mean density 500 times the critical density of the Universe at the group's redshift, and the X-ray temperatures for each potential target group using the mass–temperature relation of Sun et al. (2009). These temperatures were then used to estimate X-ray luminosities using the $L_{\rm X}$–$T$ relation derived by Slack & Ponman (2014) for archival data. As we are interested in high-entropy groups, we would expect these groups to be underluminous relative to the typical group population. Based on the simulations of McCarthy et al. (2010, 2011), we anticipated that the highest entropy groups might have X-ray luminosities suppressed by as much as a factor of 10. We therefore calculated fluxes and *Chandra* count rates assuming X-ray luminosities an order of magnitude below the mean $L_{\rm X}$–$T$ relation. From our sample of 18 potential target groups, we then selected the 10 groups with the shortest exposure times required to reach a 3$\sigma$ detection under these constraints. One of these had existing archival *Chandra* data sufficient for our purposes, and we were awarded observations of the remaining nine.

We present our selected sample in Table 1, where observed and predicted group properties have been re-estimated using data from the G3Cv06 group catalogue. Group 200130 is the well-known, relaxed X-ray group MKW4 (Fukazawa, Kawano & Kawashima 2004). This was the group with existing archival data, and was also the only group in our sample that intersected the edge of a GAMA

field. Approximately 79 per cent of the group area (within the projected radius from the dominant central galaxy to the farthest group galaxy) was covered by the survey footprint. Assuming galaxies follow a Navarro, Frenk and White (NFW) radial density profile (Navarro, Frenk & White 1996) with a concentration half that of the dark matter and using the predicted mass from Table 1, this is equivalent to missing ∼23 per cent of group galaxies within the same radius. However, as we had full coverage of the group core, we did not exclude this group from our sample.

The number of FoF galaxies within each group is shown in Table 1 for both the original G3Cv04 catalogue, on which our target list for *Chandra* observations was based, and for the deeper G3Cv06 data,[1] which has been utilized for the analysis presented in Section 3 onwards. As one would expect, the multiplicity of most groups rises somewhat with the deeper data. However, this is not guaranteed since the higher density of galaxies in G3Cv06 results in shorter linking lengths for the FoF analysis. As a result, some galaxies linked to a group in the G3Cv04 catalogue may become disconnected in G3Cv06. The most striking example of this is group 200130, which shows a substantial decrease in multiplicity from catalogue G3Cv04 to G3Cv06. Visual inspection of this group within the G3Cv04 catalogue (ID 200003 in G3Cv04) indicates that there is a substantial southern extension in the FoF group that is split off as a separate group in G3Cv06 (ID 200477 in G3Cv06 with 16 members).

Observations of the nine selected groups not already within the *Chandra* archive were completed by the ACIS-I instrument on the *Chandra X-ray Observatory* in 2013. Observations of group 200130, an ACIS-S image taken in 2002, were taken from the *Chandra* archive.

### 2.5 Group centres for X-ray analysis

Our X-ray analysis requires the location of an X-ray centre for each group, about which we will extract spectral flux (or upper limits) and, where possible, surface brightness profiles. Diffuse X-ray emission is observed in the majority of our sample, and in most cases, the centroid of this emission is coincident with a bright group galaxy. In these cases, we adopt this galaxy as the centre of the group. One group, 200115, has its X-ray emission centroid offset from any bright galaxies. For this, we adopt the X-ray centroid of the group as its centre.

Where there is no significant X-ray emission to help us locate the bottom of the gravitational potential well, we use the G3Cv06 galaxy data to define an optical group centre. For this, we adopt a slightly modified form of the iterative centring algorithm of Robotham et al. (2011). The algorithm initially takes all member galaxies and calculates a centroid weighted by galaxy luminosity. The galaxy farthest from this centre is then removed from the sample and the weighted centroid is recalculated. This procedure is iterated until only two galaxies remain, the brightest of which is then identified as the central galaxy.

We find that in a small number of cases, this can be dominated by a bright galaxy on the cluster outskirts. We modify this algorithm by assuming that central galaxies should be near the centre of the velocity distribution. The weight of each galaxy in the centroid calculation is therefore modified to include the inverse of the line-of-sight velocity offset from the group mean, scaled by the standard deviation of the velocity distribution, $|z - \bar{z}|/\sigma_z$. At each iteration, the mean velocity is recalculated whilst maintaining the standard deviation at its initial value. This modification should prevent excessively bright galaxies in the cluster outskirts dominating the weighted centroid of the group. We use this algorithm to define a central galaxy for each group. In cases where an X-ray centroid is not possible, we use this optical central galaxy as the group centroid. Ultimately, this optical centre was only required for group 200099, as explained in Section 3.5.1. The adopted centres of all 10 groups are listed in Table 1.

## 3 X-RAY ANALYSIS

In this section, we discuss the reduction and analysis of our *Chandra* data. The software packages CIAO 4.5 and SHERPA (version 1 for CIAO 4.5) were used for the data reduction and the analysis of spectra and radial profiles. The techniques used were those of Pascut & Ponman (2015), and we present only a brief outline here.

Our X-ray images were reduced from the initial level 1 event files with the calibration files from CALDB 4.5.6. These corrections include the effects of time-dependent gain variation and charge transfer inefficiency. We additionally filtered out flaring events by removing periods where the count rate was 20 per cent greater than the median rate.

The resulting cleaned event files form the basis of our X-ray analysis. We first identify point sources within our X-ray images using CIAO's WAVDETECT tool. Once these are removed, the quality of our data allows us to detect diffuse X-ray emission in most of our target groups. In groups where we do not detect significant group-scale emission, we instead calculate limits on X-ray properties as described in Section 3.5.

### 3.1 Spectral modelling

We extract the diffuse X-ray emission in the energy range 0.3–3.0 keV within a radius of $0.5r_{500}$ from our chosen centre, excluding any point sources detected in the cleaned events files. Initial estimates of $r_{500}$ are based on the GAMA luminosity-based mass estimates described previously. The extracted X-ray spectrum is fitted using a two-component source + background model. The background is separately modelled, rather than being subtracted. This allows the spectral fit to employ a maximum likelihood method using the Cash statistic (Cash 1979). This specifically allows for the Poissonian nature of the data, and so is more appropriate than $\chi^2$ for cases, such as most of ours, in which the total number of photon counts is low (Humphrey, Liu & Buote 2009).

To establish an appropriate background model we extract counts from ACIS-I chips 0-3, excluding point sources and the $0.5r_{500}$ source region. An additional CIAO routine, VTPDETECT, is used to search for any other sources of diffuse emission in the field, which are then also removed. The cleaned background region is then fitted over the range of 0.3–7.0 keV with a model that includes components for the cosmic soft X-ray and particle background, galactic emission and instrumental lines introduced by material along the optical path. We refer to Pascut & Ponman (2015) for the specifics of this fit. In a small number of cases, an additional background term is required to account for the effect of solar wind charge exchange. In these cases, we model these with a set of Gaussians corresponding to the O VII, O VIII, Ne IX and Mg XI lines at 0.56, 0.65, 0.91 and

[1] In addition to the increased depth of G3Cv06 ($r \leq 19.8$ mag compared to $r \leq 19.4$ mag for G3Cv04), the updated catalogue also re-determined all galaxy redshifts with only a small fraction of galaxies whose redshifts changed significantly. See Liske et al. (2015) for further details.

1.34 keV, respectively (Kuntz & Snowden 2008; Koutroumpa et al. 2009).

We then fit the source region as an APEC thermal plasma with the above background component. We assume a fixed metalicity of $Z = 0.5\,Z_{\odot}$ (Sanderson, O'Sullivan & Ponman 2009) relative to the GRSA cosmic abundance model (Grevesse & Sauval 1998) and take the absorption column from the galactic H I survey of Kalberla et al. (2005), extracted using the NH tool from the HEASOFT software suite.

The source + background model is then fitted. However, as the background itself consists of two components, a vignetted photon background and a non-vignetted particle background, simply rescaling the background to the source region would overcorrect the latter. We therefore fit the source in two phases, first in the range of 0.3–7.0 keV to appropriately rescale the particle background whilst providing an initial estimate of the source properties. The background component is then fixed and the source is re-fitted to determine source temperature, $T_{\rm spec}$, and APEC normalization, $\eta$, over the range 0.3–3.0 keV. The APEC model assumes $\eta = 10^{-14}/(4\pi[D_{\rm a}(1+z)]^2) \int n_{\rm e} n_{\rm H} {\rm d}V$, where $D_{\rm a}$ is the angular diameter distance to the source at redshift $z$ in cm, and $n_{\rm e}$ and $n_{\rm H}$ are the electron and hydrogen number densities (cm$^{-3}$) within a volume d$V$.

Using the fitted temperature, $T_{\rm spec}$, we then revise our estimate of $r_{500}$ using the $r$–$T$ relation of Sun et al. (2009):

$$r_{500} = 602\ h^{-1} \left( \frac{k_{\rm B} T_{\rm spec}}{3\,{\rm keV}} \right)^{1.67/3} {\rm kpc}. \quad (8)$$

The spectrum is then re-extracted within the new $0.5r_{500}$ aperture and re-fitted. If the newer estimate of $0.5r_{500}$ is larger than the initial value, then we repeat the extraction and modelling of the background, to avoid any possible contamination with diffuse source flux. We adopt the re-fitted $T_{\rm spec}$ as our estimate of the system's mean temperature and estimate group mass from this using the $M$–$T$ relation of Sun et al. (2009):

$$M_{500} = 1.27 \times 10^{14}\ h^{-1} \left( \frac{k_{\rm B} T_{\rm spec}}{3\,{\rm keV}} \right)^{1.67} {\rm M}_{\odot}. \quad (9)$$

As shown by Le Brun et al. (2014), the $M$–$T$ relation is relatively unaffected by any feedback processes. Therefore, masses estimated in this way should be representative of the halo mass regardless of the thermal history of the group (i.e. low- or high-entropy gas). In the case of groups with cool cores (CCs), the mean gas temperature will differ somewhat depending on whether or not the core region is excised when extracting the X-ray spectrum. Our data quality does not permit us to derive temperature profiles, so we do not attempt to excise core emission. However, the impact of CCs on the global spectrum has been shown to be small. Rasmussen & Ponman (2007) show in their *Chandra* study that the central temperature in groups drops only 10–20 per cent below the mean group temperature, even in systems with strongly cooling cores (see their fig. 6), and Osmond & Ponman (2004) find that the impact of core excision on the mean spectral temperature of groups is only ≈4 per cent. In practice, as we discuss in Section 4.2, with the exception of MKW4, our groups seem likely to contain at most very weak CCs.

### 3.2 Surface brightness profiles

The surface brightness profiles of our groups are extracted by binning the observed emission in annuli centred on the positions listed in Table 1. Bin widths are chosen to give at least 15 counts per bin in our 0.3–3.0 keV energy band. We remove contaminating point sources and apply an exposure correction. For groups without any strong CC, we assume that the surface brightness profile can be represented by a single $\beta$-model (Cavaliere & Fusco-Femiano 1976):

$$S(r) = S_0 \left( 1 + \left( \frac{r}{r_{\rm c}} \right)^2 \right)^{-3\beta+0.5}, \quad (10)$$

where $r_{\rm c}$ is the core radius, $\beta$ determines the slope of the emission profile and $S_0$ is the central surface brightness. In groups with a noticeable excess of central emission, we modify the surface brightness model to be the sum of two $\beta$-models, $S(r) = S_{\rm core}(r) + S_{\rm out}(r)$. This modification is simpler than those used by, for example, Ettori (2000) and Vikhlinin et al. (2006). Due to the limited quality of the data from most of our groups, fitting more complex models is unlikely to provide significant improvements.

A flat background component, $S_{\rm bg}$, is incorporated into the fitted surface brightness model. This is not strictly correct, since the particle background is not subject to vignetting, unlike the photon background, so after exposure correction (which flattens the photon component of the background), the particle contribution will actually rise with radius from the optical axis of the instrument. However, as most of our sources do not cover a very large fraction of the ACIS-I field (radial extent typically less than or approximately a few hundred pixels compared to a 2048-pixel-wide field of view), and as our energy range does not extend into the hard X-ray regime where particles dominate the background, departures from a uniform background will be small.

The surface brightness profiles are fitted using SHERPA. Due to limited statistics, we do not fit all $\beta$-model components, we fix $\beta_{\rm out} = 0.5$, comparable to that observed for low-temperature groups (e.g. Helsdon & Ponman 2000), and $\beta_{\rm core} = 2/3$, assuming that central emission has a standard slope comparable to those measured in Mohr, Mathiesen & Evrard (1999).

### 3.3 Luminosity

To determine the bolometric X-ray luminosity of the diffuse group emission, we use the spectral fit and the SHERPA algorithm CALC_ENERGY_FLUX in the energy range 0.01–15 keV, applying the appropriate conversion from flux to luminosity. As our extraction aperture is smaller than $r_{500} - 0.5r_{500}$ in most cases – we estimate the luminosity, $L_{\rm X,\,500}$, within $r_{500}$ by applying a rescaling based on the measured surface brightness profile. The rescale factors typically range from 1.12 to 1.75. One group, 300067, requires little rescaling (1.04) due to its centrally concentrated emission profile, whilst the three groups 100053, 200099 and 200130, for which the extraction aperture is only 100 kpc (see Section 3.5), have larger scalefactors of 3–6.

### 3.4 ICM entropy

We define entropy, $K$, as

$$K(r) = \frac{k_{\rm B} T_{\rm spec}}{n_{\rm e}(r)^{2/3}}, \quad (11)$$

where we assume isothermal gas with temperature $T_{\rm spec}$ and $n_{\rm e}(r)$ is the number density of electrons in the intragroup gas at radius $r$ (Voit, Kay & Bryan 2005). We note that the assumption of an isothermal gas can lead to slight overestimates of central entropy in systems with CCs. To determine the gas density, follow the method

of Hudson et al. (2010) to deproject $\beta$-model fits to the surface brightness profile. For the single $\beta$-model, this defines

$$n_{\rm e}(r) = n_{\rm e,0}\left(1+\left(\frac{r}{r_{\rm c}}\right)^2\right)^{-3\beta/2}, \quad (12)$$

where $\beta$ and $r_{\rm c}$ are derived from the surface brightness profile (equation 10), and $n_{\rm e,\,0}$ is a normalization factor calculated as

$$n_{\rm e,0} = \sqrt{\frac{n_{\rm eH} 4\pi D_{\rm a}(z)^2 (1+z)^2 10^{14} \eta J}{\rm EL}}. \quad (13)$$

Here $n_{\rm eH} = 1.176$ is the ratio of electron to hydrogen number densities within a fully ionized plasma of $0.5\,{\rm Z}_{\odot}$ metallicity [relative to the GRSA (Grevesse & Sauval 1998) abundance tables] and $D_{\rm a}(z)$ is the angular diameter distance to the group in cm at redshift $z$. $\eta$ is the normalization of the APEC model fit in Section 3.1 and EL is the ratio of the emission integral within our extracted region to the central electron density.

Equation (12) can be extended to a double $\beta$-model fit as

$$n_{\rm e}(r)^2 = n_{\rm e,0,core}^2\left(1+\left(\frac{r}{r_{\rm c,core}}\right)^2\right)^{-3\beta_{\rm core}} + n_{\rm e,0,out}^2\left(1+\left(\frac{r}{r_{\rm c,out}}\right)^2\right)^{-3\beta_{\rm out}}, \quad (14)$$

where the labels 'core' and 'out' indicate the relevant property from the core and outer $\beta$-model fit. We refer to Hudson et al. (2010) for the calculation of the central electron densities $n_{\rm e,\,0}$, $n_{\rm e,\,0,\,core}$ and $n_{\rm e,\,0,\,out}$.

Using the derived gas density profile and equation (11), we calculate the gas entropy at a radius of 10 kpc in each group to probe the core gas properties.

### 3.5 Notes on individual groups

Some of the groups within the sample required modification to some aspects of our standard analysis procedure. These are described below.

#### *3.5.1 100053 and 200099*

Since their surface brightness profiles show no significant X-ray emission on group scales, groups 100053 and 200099 are considered to be non-detections, and we instead derive limits on the gas luminosity and entropy.

Examining the smoothed emission maps of these sources, we find a small diffuse source associated with a bright member galaxy for 100053 (see Fig. 1) and adopt this galaxy as the centre of our analysis. 200099 appears featureless in the smoothed images. We therefore adopt an optical centre for this group based on the iterative centroid algorithm described in Section 2.5, though we note that the centre identified by the algorithm in this case actually lies near the edge of the group.

To determine limits on the gas properties for these two systems, we extract X-ray spectra within 100 kpc, using a small, fixed aperture to increase the signal-to-noise ratio relative to that within $0.5r_{500}$. Assuming the $T_{\rm pred}$ determined from the optical group luminosity, we fit an APEC model with a fixed temperature and metallicity. We then adopt an upper limit corresponding to the $2\sigma$ upper bound on the fitted APEC normalization $\eta$. The surface brightness profile is taken to be a single $\beta$-model with $\beta = 0.5$ and $r_{\rm c} = 0.2r_{500}$, comparable to the mean of the other eight groups in the sample ($0.17 \pm 0.03\,r_{500}$). We assume $r_{500}$ as predicted by the luminosity mass estimate.

Using the $2\sigma$ upper limit on normalization and the assumed surface brightness profile, a $2\sigma$ upper limit on luminosity can be derived. Deprojecting this surface brightness profile provides a $2\sigma$ upper limit on electron number density, $n_{\rm e}$. Combining this with the assumed gas temperature, $T_{\rm pred}$, gives a $2\sigma$ *lower* limit on central entropy.

#### *3.5.2 200130*

Group 200130 is the known low-redshift X-ray group MKW4 (Fukazawa et al. 2004). This group was imaged in 2002 with *Chandra* in the ACIS-S configuration. We extract our spectra from the back-illuminated S3 chip. However, due to the low redshift of this group, the predicted $0.5r_{500}$ aperture we would ordinarily use (313 kpc, 6.7 arcmin at $z = 0.02$) extends beyond the chip boundary. Additionally, this system is known to have traceable emission across the ACIS-S CCD (Sun et al. 2009), rendering our usual approach of measuring a local background unsuitable.

We instead use the Markevitch blank sky background data sets to estimate the background (Vikhlinin et al. 2005; Sun et al. 2009). Using the S3 chip only, we extract a spectrum within a 100 kpc aperture, comparable to the size of the chip. We do this for both the background and data. We scale the background to match the hard X-ray counts and subtract this from our source spectrum. We then fit with a source model using a $\chi^2$ statistic.

To determine the radial profile, as we do not have data beyond 100 kpc, we again make use of the scaled blank sky background to constrain background emission. We use the core radius and slope of the outer gas halo, $r_{\rm c} = 204$ kpc and $\beta = 0.64$, determined by Vikhlinin, Forman & Jones (1999), using *ROSAT* imaging data that extended to a much larger radius. We perform two $\beta$-profile fits of the background-subtracted radial profile where we fit only the amplitude of the outer $\beta$ model but allow the inner, core profile freedom to optimize normalization, core radius and slope.

We calculate luminosity as described previously, extrapolating from 100 kpc to $r_{500}$. Profiles of temperature for this group are available from the literature (e.g. Vikhlinin et al. 2006; Sun et al. 2009). However, for consistency with the treatment of our other groups, we adopt a single mean temperature, $T_{\rm spec}$, calculated from an emission-weighted temperature profile. We use the temperature profile from Vikhlinin et al. (2006) and, weighting by the surface brightness profile, average within $0.5r_{500}$, adopting $r_{500} = 538$ kpc initially (Sun et al. 2009). This temperature is then used to recalculate $r_{500}(T)$, and the mean temperature is recomputed, iterating until convergence. The final mean temperature is used for our entropy estimate.

#### *3.5.3 200115*

Group 200115 features a diffuse X-ray source not associated with any member galaxy. There are no background groups or clusters in the GAMA survey that this emission may be associated with, nor are any known groups or clusters within 1 arcmin of the emission found within the NASA Extragalactic Database.[2] We therefore attribute

[2] The NASA/IPAC Extragalactic Database (NED) is operated by the Jet Propulsion Laboratory, California Institute of Technology, under contract with the National Aeronautics and Space Administration.

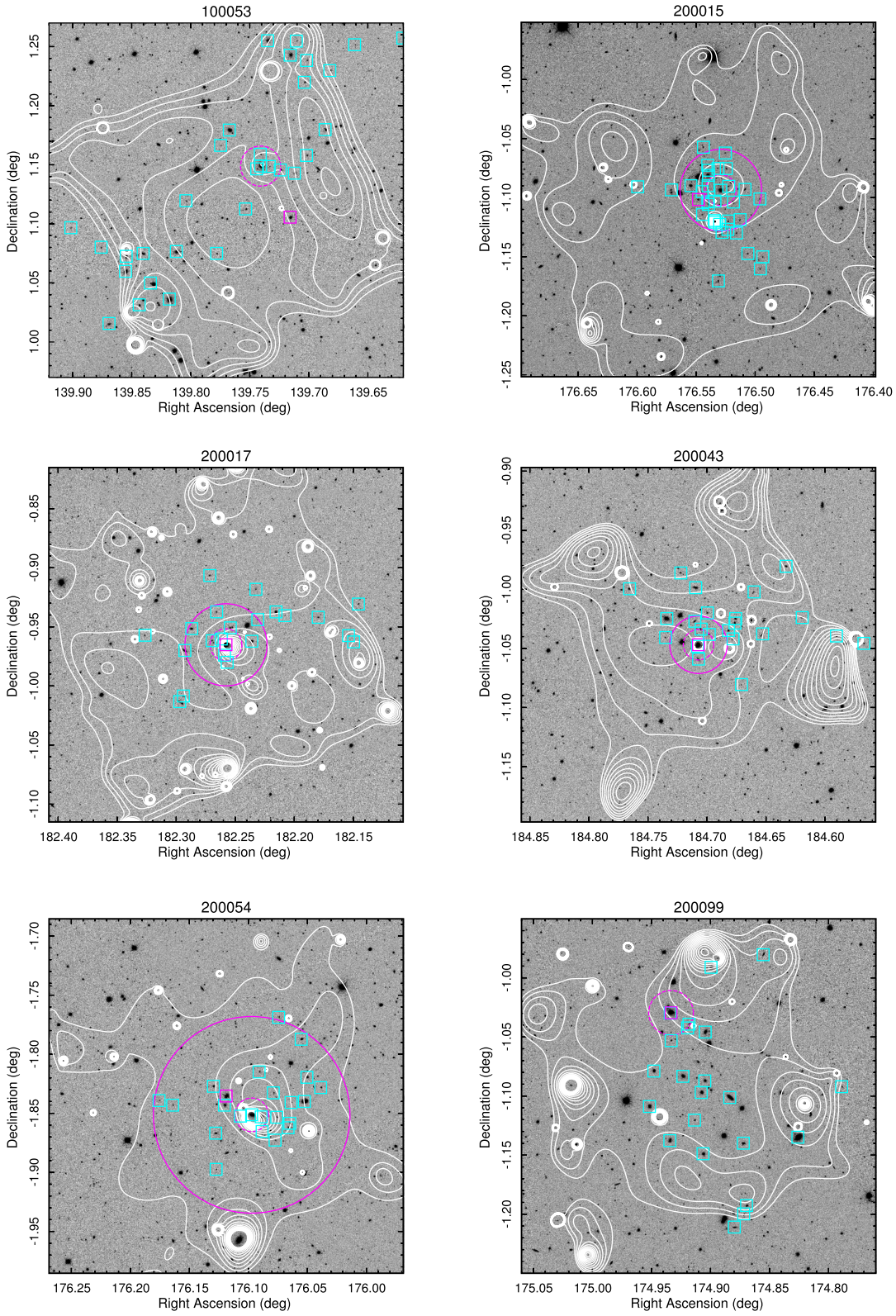


**Figure 1.** Optical images of our groups from the SDSS with X-ray contours overlaid (white lines). The X-ray contours are derived from adaptively smoothed images of the observed X-ray emission in our analysis band (0.3–3.0 keV) set at arbitrary levels for illustration purposes only. Also shown are the G3Cv06 member galaxies (cyan squares) with central galaxies (as defined by our iterative centre-of-light algorithm defined in Section 2.5) marked by magenta squares. For scale, we illustrate a 100-kpc region with a dashed magenta circle and the extraction region, when different, by the solid magenta circle centred on the X-ray source to be analysed (either the X-ray centroid or an optical centre; see Section 2.5).

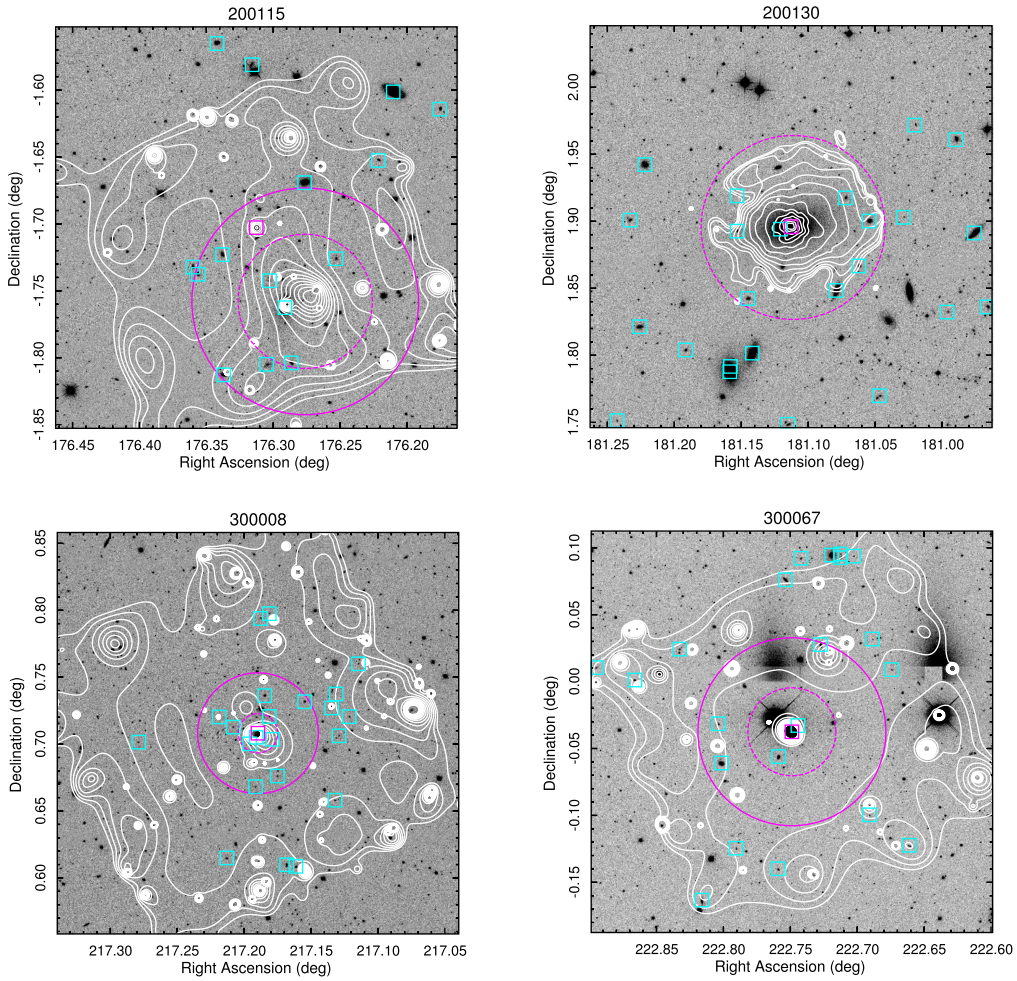


**Figure 1** – *continued*

the emission to the group, and estimate its centroid in the 0.3–3.0 keV band within a 100-kpc aperture (at $z = 0.028$), finding this to be offset by 130 kpc from the central galaxy identified by our iterative centre-of-light algorithm. Another bright galaxy, only 0.05 mag fainter, is offset by 32 kpc from the X-ray centroid. We note that such offsets have been seen in other groups and clusters that appear to have been subject to recent disturbance. We use the X-ray centroid as the centre for our subsequent analysis.

### *3.5.4 200054*

Fitting the spectrum of group 200054 over our standard 0.3–3.0 keV band, we find a high temperature of $5.2^{+4.9}_{-1.9}$ keV. This motivates us to extend the upper energy band, whereupon the fitted temperature drops substantially to ∼3 keV. We therefore opt to fit this group within the full 0.3–7.0 keV band used when rescaling the background. We additionally take $\beta_{\rm out} = 2/3$, consistent with high-temperature systems, rather than the lower value, $\beta_{\rm out} = 0.5$, used for the cooler groups within this work.

### *3.5.5 300067*

The emission within this group was observed to be highly centrally concentrated. Attempting to fit the two $\beta$-models to the surface brightness profile found a negligible contribution from the second, outer $\beta$-model. We instead fit a single profile.

## 4 RESULTS

In this section, we present the results for our sample of optically selected galaxy groups. The results of the spectral fitting and derived properties are shown in Table 2, whilst Table 3 presents the results of the surface brightness fits to each group. Diffuse X-ray emission is detected in 8 of our 10 groups, a larger fraction than detected in studies such as the XI project (only one bright source and two weak detections out of nine targets; Rasmussen et al. 2006) where substructure/virialization was not considered when selecting groups. Our detected fraction is consistent with that found in the optically selected groups studied by Balogh et al. (2011), who found that five groups were undetected in a sample of 18 targets. Interestingly, their sample, which was drawn from the 2PIGG catalogue (Eke et al. 2004) with a narrow mass range ($3 \times 10^{14} < M/{\rm M}_{\odot} < 6 \times 10^{14}$), was additionally selected to exclude groups with non-Gaussian velocity distributions. Whilst these samples are small, the difference between the XI result and that presented here does indicate that selection by substructure can substantially improve the reliability of a group sample.

In Fig. 1, we show the optical SDSS images with X-ray contours overlaid. Of the eight groups where we detect X-ray

**Table 2.** Results of the X-ray analysis for our sample of optically selected groups.

| GroupID | $T_{\rm spec}{}^a$ (keV) | $L_{\rm X,500}{}^b$ ($10^{42}$erg s$^{-1}$) | $M_{500}{}^c$ ($10^{13}M_\odot$) | $r_{500}{}^c$ (kpc) | $K_{10\,\rm kpc}$ (keV cm$^2$) | $f_{500,\rm gas}{}^d$ |
|---|---|---|---|---|---|---|
| 100053 | (1.53) | <1.70 | (5.91) | (576) | >267 | <0.026 |
| 200015 | $1.05^{+0.21}_{-0.12}$ | 3.02 ± 0.66 | 3.16 ± 0.83 | 480 ± 42 | 52.9 ± 13.7 | 0.045 ± 0.007 |
| 200017 | $1.34^{+0.56}_{-0.23}$ | 1.36 ± 0.46 | 4.74 ± 2.33 | 550 ± 90 | 52.7 ± 11.9 | 0.025 ± 0.003 |
| 200043 | $0.97^{+0.37}_{-0.25}$ | 1.63 ± 0.62 | 2.77 ± 1.47 | 460 ± 81 | 45.1 ± 20.6 | 0.034 ± 0.008 |
| 200054 | $2.80^{+1.03}_{-0.53}$ | 12.5 ± 1.61 | 16.2 ± 7.53 | 828 ± 129 | 110 ± 80.0 | 0.037 ± 0.010 |
| 200099 | (1.34) | <1.24 | (4.71) | (536) | >243 | <0.025 |
| 200115 | $0.59^{+0.09}_{-0.10}$ | 0.37 ± 0.06 | 1.20 ± 0.12 | 347 ± 30 | 64.5 ± 20.6 | 0.024 ± 0.004 |
| 200130 | $1.79^{+0.02}_{-0.02}$ | 27.2 ± 0.6 | 7.66 ± 0.15 | 645 ± 4 | 26.9 ± 0.4 | 0.075 ± 0.002 |
| 300008 | $1.67^{+0.31}_{-0.23}$ | 1.99 ± 0.30 | 6.80 ± 1.83 | 620 ± 56 | 97.7 ± 38.4 | 0.023 ± 0.004 |
| 300067 | $0.90^{+0.11}_{-0.08}$ | 0.39 ± 0.06 | 2.44 ± 0.44 | 440 ± 27 | 35.8 ± 4.9 | 0.008 ± 0.001 |

Values in parentheses are derived from GAMA mass and temperature estimates.
[a]Mean temperature within an aperture of $\approx 0.5 r_{500}$.
[b]Extrapolated using the surface brightness fits from the extraction aperture to $r_{500}$.
[c]Derived from the Sun et al. (2009) mass–temperature and radius–temperature relations for groups and clusters.
[d]Estimated gas mass fractions within $r_{500}$ (Section 4.3).

**Table 3.** X-ray surface brightness profiles.

| GroupID | $r_{\rm c,\,core}{}^a$ (kpc) | $\beta_{\rm core}{}^a$ | $r_{\rm c,\,out}{}^a$ (kpc) | $\beta_{\rm out}{}^a$ |
|---|---|---|---|---|
| 100053 | – | – | (115) | (0.5) |
| 200015 | 18 ± 17 | (0.66) | 107 ± 31 | (0.5) |
| 200017 | 10 ± 6 | (0.66) | 77 ± 28 | (0.5) |
| 200043 | 14 ± 23 | (0.66) | 87 ± 48 | (0.5) |
| 200054 | 25 ± 33 | (0.66) | 160 ± 24 | (0.66) |
| 200099 | – | – | (107) | (0.5) |
| 200115 | – | – | 36 ± 49 | (0.5) |
| 200130 | 4.0 ± 0.8 | 0.444 ± 0.004 | $(204)^b$ | $(0.64)^b$ |
| 300008 | 9.4 ± 19.1 | (0.5) | 88 ± 15 | (0.66) |
| 300067 | 15 ± 4 | (0.66) | – | – |

[a]Surface brightness profiles assuming the double $\beta$-model described in Section 3. In cases of non-detection or where only one $\beta$-model is sufficient, we report only one set of model parameters. Values in parentheses are fixed as described in the text and not allowed to fit.
[b]Outer surface brightness profile parameters derived by Vikhlinin et al. (1999) from a fit to the *ROSAT* PSPC data.

emission, there are three groups (200015, 200054 and 200115) where the central galaxy identified by our iterative centre-of-light algorithm (Section 2.5) is not associated with the peak of the X-ray emission.

### 4.1 $L_{\rm X}$–$T_{\rm spec}$

An initial assessment of our sample can be made through their position on the X-ray luminosity–temperature relation (*L*–*T*). This relation, which has a self-similar expectation of $L_{\rm X} \propto T^2$ for systems with temperatures above ∼3 keV, and a flatter slope at lower temperatures ($L_{\rm X} \propto T$; Balogh, Babul & Patton 1999) where line emission is significant, has been shown to be significantly steeper, especially in the group regime (e.g. Helsdon & Ponman 2000; Osmond & Ponman 2004; Pratt et al. 2009; Slack & Ponman 2014), with slopes of 3 to 4. This similarity breaking is attributed to feedback processes that inject entropy into the gas halo (e.g. Balogh et al. 1999; Babul et al. 2002; Voit & Bryan 2001), suppressing X-ray luminosity in gas cores.

In Fig. 2, we show our group sample overplotted on the *L*–*T* group data from the GEMS sample of Osmond & Ponman (2004).

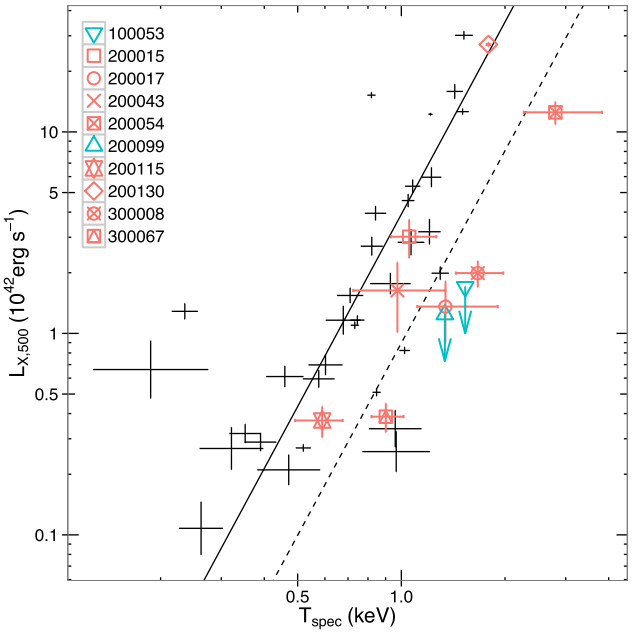


**Figure 2.** The *L*–*T* relation for our group sample (coloured points). Overlaid are groups from the Osmond & Ponman (2004) sample (black points). The solid line represents the *L*–*T* relation of Slack & Ponman (2014). We show the *L*–*T* relation of our sample, modified from the Slack & Ponman (2014) relation by re-fitting the normalization only, excluding the undetected groups 100053 and 200099, as the dashed line.

Also shown is the *L*–*T* relation (for groups only) found by Slack & Ponman (2014) using a compilation of several group and cluster studies spanning nearly two orders of magnitude in temperature:

$$L_{\rm X,500} = 1.27 \times 10^{44} \left( \frac{k_{\rm B} T}{3\,\rm keV} \right)^{3.17} \rm erg\,s^{-1}. \quad (15)$$

With the exception of the archival group MKW4 (200130), we find that our groups have X-ray luminosities below those observed for the GEMS sample and expected from the *L*–*T* relation for typical X-ray group samples. Quantifying the size of our luminosity decrement relative to the literature *L*–*T* relation by fitting the

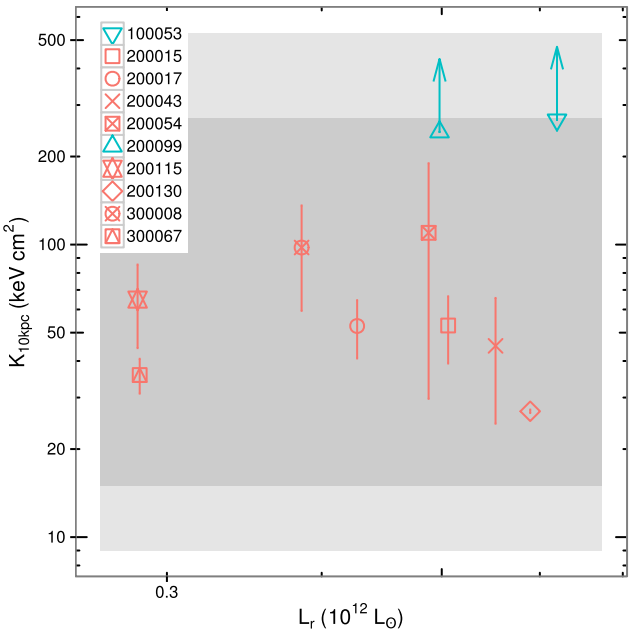


**Figure 3.** Central (10 kpc) entropies against total optical *r*-band luminosity. We show the $1\sigma$ (dark shading) and $2\sigma$ (light shading) upper and lower limits at 10 kpc derived from the OWLS simulations (McCarthy et al. 2011).

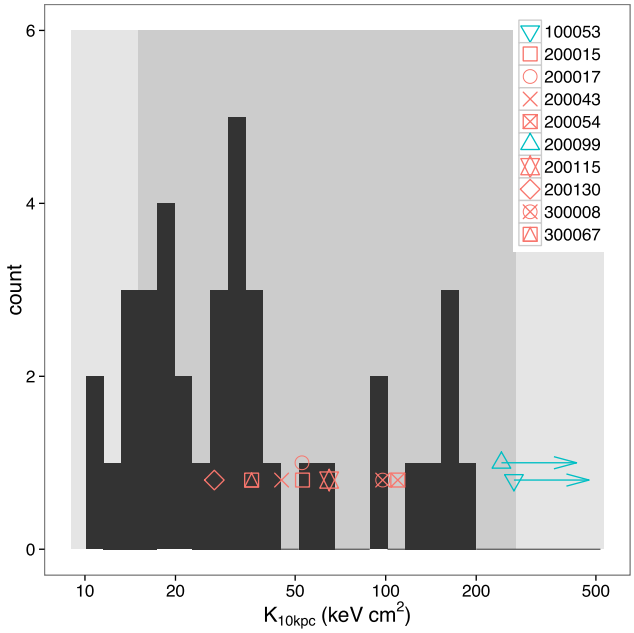


**Figure 4.** Histogram of group entropies at 10 Kpc using the entropy profiles of the ACCEPT sample (Cavagnolo et al. 2009) with $k_BT < 3$ keV with our measured entropies overlaid. As in Fig. 3, we show the $1\sigma$ (dark shading) and $2\sigma$ (light shading) upper and lower limits at 10 kpc derived from the OWLS simulations (McCarthy et al. 2011).

normalization of the relation to our data (excluding the two non-detections), we find that our optically selected sample is underluminous by a factor of 4 relative to an X-ray-selected one. This renormalization is shown as the dashed line on Fig. 2. This deficit is in qualitative agreement with the results of Anderson et al. (2015), who find optical groups in a stacked analysis to be a factor of 2 underluminous on the *L–M* relation.

Despite the group luminosities being low compared to the standard relation, our measured group temperatures show no significant bias relative to temperatures predicted from the optical luminosity-based mass estimates using the Sun et al. (2009) *M–T* relation. Excluding the two non-detections, and MKW4, whose analysis differed from that of the other groups, the mean offset between predicted and observed temperatures $[\log_{10}(T_{\rm pred}) - \log_{10}(T_{\rm spec})]$ is only $-0.005 \pm 0.072$, increasing slightly to $-0.007 \pm 0.062$ if MKW4 is included. This suggests that the mass estimation used here is, on average, unbiased, though with substantial scatter. This scatter, totalling 0.18 dex, has 0.09 dex contributed by the measurement error on $T_{\rm spec}$, with the remaining 0.15 dex introduced through uncertainty on the calibration of the optical luminosity mass estimation and intrinsic scatter on that relation.

### 4.2 Entropy

In Fig. 3, we plot central entropies, calculated from equation (11) using the surface brightness parameters in Table 3 to estimate gas density, against optical luminosity. We plot against $L_r$ to avoid any correlation that may be introduced by plotting against an X-ray-derived quantity. Note that the group sample spans a fairly narrow range in $L_r$, as a result of the selection on richness and predicted *Chandra* exposure time. This is not a problem for our study, since we are effectively exploring the full range in gas properties for groups over a limited mass range. In the OWLS project simulations, the feedback model that best reproduces the observed entropy distribution, as well as other halo baryon properties such as stellar mass fractions, incorporates both AGN and supernova feedback, together with radiative cooling (McCarthy et al. 2011). The predicted range in central entropies from this model is shown in Fig. 3 by the shaded regions. The majority of our groups lie well within the $1\sigma$ range; however, we note that our two non-detections have $2\sigma$ lower limits substantially higher than the central entropies of the rest of the sample. These two groups are plausible candidates for members of the population of high-entropy groups predicted by the strong feedback models.

In Fig. 4, we compare these results to the distribution of central entropies for groups and clusters within the ACCEPT (Cavagnolo et al. 2009) data base.[3] We use entropy profiles $K(r) = K_0 + K_{100}(r/100\,{\rm kpc})^\alpha$ with their fitted values of $K_0$, $K_{100}$ and $\alpha$ to estimate group entropies at 10 kpc. For comparability with our sample, we have taken only groups with $T_{\rm X} < 3$ keV, which reduces the ACCEPT sample from 241 systems to 38. The estimated entropies at 10 kpc for our X-ray detected systems mostly lie above the main peak in the entropy distribution for the Cavagnolo et al. (2009) sample, and a two-sided Kolmogorov–Smirnov test gives a low probability ($p = 0.04$) that the two distributions are consistent. The sense of this disagreement, whereby the majority of our entropy estimates appear elevated relative to the general ACCEPT population, is consistent with the lower X-ray luminosity observed. Moreover, the high-entropy group candidates, 100053 and 200099, have lower limits on entropy, which are higher than the largest central entropies seen in the cool ACCEPT sample.

Since MKW4 (our group 200130) is included in ACCEPT, we can compare the value of entropy in this derived from our own analysis with that calculated from the Cavagnolo et al. (2009) data. As shown in Table 2, we determine a central entropy of $26.9 \pm 0.4$ keV cm$^2$, compared to the value of 28.4 keV cm$^2$ derived from the ACCEPT profile. Whilst the ACCEPT value lies outside our small $1\sigma$ confidence region, this small error bar results from the high statistical quality of the data for this particular system. (As can

[3] http://www.pa.msu.edu/astro/MC2/accept/

be seen from the table, entropy errors for all other groups in our sample are at least an order of magnitude larger.) In practice, much larger discrepancies can be expected to follow from the simplicity of our method (the isothermality assumption, for example, compared to the temperature deprojection used for ACCEPT), so we regard agreement to ∼5 per cent as quite satisfactory.

To estimate the lower limits on group entropy for groups 100053 and 200099, a series of assumptions needed to be made regarding the temperature and gas density profiles. We investigate these assumptions and the impact deviations from them might have on the estimated limits in Section 5.

As entropy and cooling times are inherently linked properties of group gas (at the same temperature, high gas entropy implies low gas density and therefore a reduced cooling rate), we can use our measured entropies to explore the CC/non-cool core (NCC) status of the groups in our sample. Our choice of the threshold separating these two populations is guided by the observed bimodality in central entropies reported by Cavagnolo et al. (2009), which split the population at 30–50 keV cm$^2$. Groups below this threshold were found to be more likely to show features associated with active cooling (Cavagnolo et al. 2008). Whilst the Cavagnolo et al. (2009) split is based on the value of the central baseline value ($K_0$) derived from fitting the $K(r)$ model discussed above, our radius of 10 kpc should be small enough for the entropy to have dropped close to the baseline value, so it is reasonable to adopt a similar threshold value. Accordingly, we classify groups with $K_{10\mathrm{kpc}} < 30\,\mathrm{keV\,cm^2}$ as containing probable CCs.

From Table 2, we see that only one group falls below this threshold and is therefore likely to be a CC group. Though two of our groups are plausibly moderate NCC groups, with central entropies lying just above or consistent within $1\sigma$ of the CC threshold, the remainder of our sample, though consistent with the CC threshold at a $2\sigma$ level, are likely NCC groups. Cooling times can be estimated as $t_{\mathrm{cool}} \propto K^{3/2}T^{-1/2}\Lambda(T)^{-1}$, where $\Lambda(T)$ is the cooling function. For pure bremsstrahlung emission where $\Lambda(T) \propto T^{1/2}$ (e.g. Donahue et al. 2006), this results in $t_{\mathrm{cool}} \propto K^{3/2}T^{-1}$. At low temperatures where line emission becomes significant, such as in the groups observed here, the temperature dependence of $\Lambda(T)$, and hence of $t_{\mathrm{cool}}(T)$ flattens (e.g. McKee & Cowie 1977; Balogh et al. 1999). With the exception of group 200130, which has the second highest temperature, three of our four lowest entropy groups are also amongst the coolest groups in this sample and should therefore have the lowest cooling times.

We note that in the case of group 300067, the diffuse X-ray emission is confined to a small region around a central galaxy. This is reminiscent of the compact galaxy coronae observed by Sun et al. (2007). Its radial extent (∼15 kpc) is larger than those seen by Sun et al. (2007) (∼4 kpc), but its temperature is comparable. The Sun et al. (2007) coronae were found around galaxies within hot cluster environments. This clearly differs from the environment seen in 300067, where no other diffuse emission is observed. It is possible that this compact X-ray halo is surrounded by undetectable high-entropy gas, but we do not label this group as a high-entropy candidate.

### 4.3 Gas mass fraction

Using the gas number density profiles determined above, $n(r)$, we can also determine the gas mass fractions for each group. We follow the method of Sanderson et al. (2013) such that

$$M_{500}^{\mathrm{gas}} = m_{\mathrm{e}} \int_0^{r_{500}} 4\pi r^2 n_{\mathrm{e}}(r)\,\mathrm{d}r, \qquad (16)$$

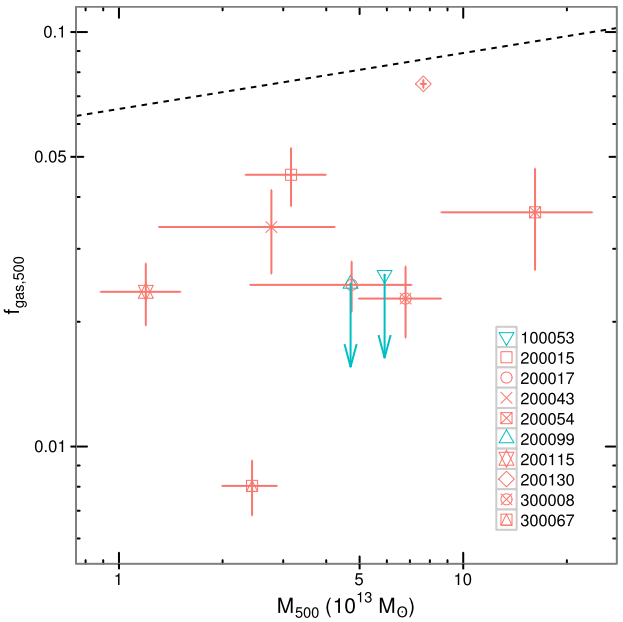


**Figure 5.** Gas mass fraction within $r_{500}$ for our 10 groups. Colour code and key as per Fig. 2, with blue points indicating the groups for which only a $2\sigma$ upper limit on gas mass has been determined. For comparison, the dashed line indicates the best-fitting $f_{500}^{\mathrm{gas}}-M_{500}$ relation found by Sun et al. (2009) for their sample of X-ray-selected groups and clusters.

where the factor $m_{\mathrm{e}} = 1.159$ amu is the gas mass per electron (1 amu $= 1.66 \times 10^{-27}$ kg) for a fully ionized plasma of $0.5\,\mathrm{Z}_{\odot}$ metallicity [again, relative to the GRSA (Grevesse & Sauval 1998) abundance tables]. For groups 100053 and 200099, we determine a $2\sigma$ upper limit on gas mass using the standard $\beta$ model and parameters estimated from GAMA optical data and limits from the X-ray data. The resulting upper limits on the gas mass fractions are shown in Fig. 5 and in Table 2.

As might be expected from the low X-ray luminosity of our systems, their gas mass fractions are found to be almost universally low compared to those seen in X-ray-selected systems, which typically find $f_{\mathrm{gas}} \sim 0.06$–$0.08$ within our mass range of $10^{13}$–$10^{14}\,\mathrm{M}_{\odot}$ (Sun et al. 2009; Gonzalez et al. 2013; Liang et al. 2016). Within our sample, only group 200130 (MKW4) has such a substantial gas reservoir.

## 5 DISCUSSION

### 5.1 High-entropy limits

The results above indicate that two of our groups have interestingly high lower limits on the central entropy of their intragroup gas. However, it is worth asking how realistic these limits are, especially given the assumptions that have gone into constructing them. The entropy calculation used here for the detected systems assumes an isothermal gas with temperatures determined from the X-ray spectra, and a gas density profile derived from the deprojected emissivity profile of group emission. To determine limits for the undetected groups, we instead use the temperature predicted for each group from their optical luminosity-based masses, which have some uncertainty from the scatter in the mass–$L_r$ relation used. The uncertainty on mass also affects the shape of the density profile, since we assume $r_{\mathrm{c}} = 0.2r_{500}$, where $r_{500}$ is also derived from optical luminosity-based masses. Furthermore, the assumed factor of 0.2,

**Table 4.** Substructure in the G3Cv06 group sample.

| GroupID | $\zeta_\beta$ | $\zeta_{\rm AST}$ | $\zeta_{\rm AD}$ |
|---|---|---|---|
| 100053 | 1.42 (0.93) | 1.19 (0.70) | 2.39 |
| 200015 | 1.22 (0.81) | 0.82 (0.23) | 1.11 |
| 200017 | 1.06 (0.63) | 1.39 (0.78) | 3.97 |
| 200043 | 1.86 (>0.99) | 2.40 (0.98) | 1.44 |
| 200054 | 0.78 (0.26) | 1.24 (0.69) | 3.41 |
| 200099 | 3.08 (>0.99) | 2.08 (0.95) | 2.19 |
| 200115 | 1.43 (0.89) | 1.42 (0.76) | 1.03 |
| 200130 | 1.78 (0.99) | 1.23 (0.74) | 3250 |
| 300008 | 1.11 (0.68) | 0.79 (0.21) | 1.03 |
| 300067 | 1.55 (0.94) | 1.93 (0.93) | 2.86 |

*Notes.* $\zeta_\beta$, $\zeta_{\rm AST}$ and $\zeta_{\rm AD}$ show the mirror symmetry, angular separation test and velocity non-normality substructure indicators, as described in Section 2. The numbers in parentheses show the significance of any observed substructure for the first two tests.

comparable to the mean ratio of $r_{\rm c}$ to $r_{500}$ for the rest of the sample, may not be valid for groups with such high entropy – high-entropy gas will redistribute itself within the halo, puffing up the intragroup medium and increasing the core radius.

It is interesting therefore to see how far we can push these assumptions before we reach entropy limits comparable to the rest of the sample. The most obvious question is: How reliably do we know the assumed temperature? We have already discussed that, for the detected systems, the temperature estimates are, on average, essentially unbiased. Whilst scatter is large, 0.15 dex, if we decrease the temperature by 0.15 dex and propagate this change into $r_{\rm c}$, entropy lower limits decrease to only $>181$ and $>164\,{\rm keV\,cm^2}$ for 100053 and 200099, respectively. Therefore, poorly estimated temperature alone cannot be responsible for the observed high-entropy limits.

The second main assumption involved in our calculation of the entropy at 10 kpc radius is the form of the gas density profile. The key parameter here is the value of the core radius, which was assumed to take the value $0.2r_{500}$. We therefore examine the fraction of $r_{500}$ that would be required to reduce the measured limits at 10 kpc to $100\,{\rm keV\,cm^2}$. From our APEC normalization upper limit, we find that this core radius would need to drop to $<0.05r_{500}$ for both groups, giving entropy profiles that drop sharply at small radius. This seems highly unlikely for a group with undetectable low X-ray surface brightness. As we noted earlier, if such a group contains high-entropy gas, then the core radius is likely to take a *larger* than normal value.

### 5.2 Substructure

We conclude from the above discussion that the high-entropy limits determined for 100053 and 200099 are unlikely to be reduced substantially by adjustments to our assumptions about the gas temperature or density. However, a third possibility remains to avoid the conclusion that these systems contain high-entropy gas. Could it be that the gas in these systems has not yet been heated, since they are still collapsing? Our initial dynamical screening was, of course, designed to eliminate this possibility. Given the improvement in optical data quality since the initial selection of our group sample using the G3Cv04 GAMA catalogue, we now re-visit the question of substructure for the whole sample using the G3Cv06 data.

In Table 4, we show the recalculated substructure statistics of our group sample using the deeper data now available and centred on X-ray emission where possible. We remind the reader that the original G3Cv04 substructure thresholds were $\zeta_\beta < 1.9$, $\zeta_{\rm AST} < 1.68$ and $\zeta_{\rm AD} < 1.82$. Our target groups all fell below these threshold values using the G3Cv04 galaxy data. Due to the updated group catalogue, a rigorous comparison of the new substructure statistics to the original, carefully calibrated, thresholds is difficult, and would require recalibration of these thresholds using mock data sets constructed to match the deeper data. Qualitatively though, such a comparison has a number of interesting implications.

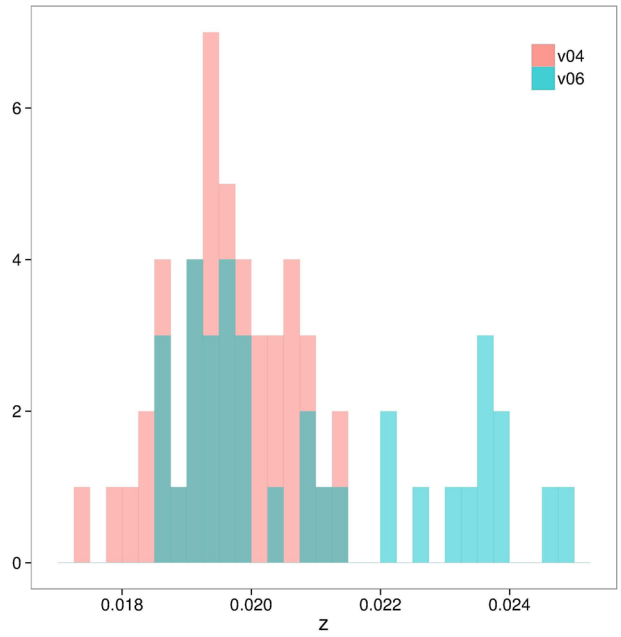


**Figure 6.** Histogram of galaxy redshifts for members of group 200130 (MKW4) identified within G3Cv04 (red) and G3Cv06 (blue) group catalogues. A large fraction of the galaxies linked to this group in G3Cv04 are part of another group in G3Cv06 (see the text and Section 2.4).

The most apparent change is that the AD-test has become much more discriminating. Obviously, the inclusion of more galaxies will result in any deviation from normality in the velocity distribution becoming more significant, so this should not surprise us. However, the value of $\zeta_{\rm AD} = 3250$ for 200130 (MKW4) indicates that the revised selection has introduced a major perturbation in its velocities. Further examination indicates that a second structure, centred at $z \sim 0.0235$, has been linked into the group in the G3Cv06 catalogue, causing the group velocity histogram to be significantly skewed, as shown in Fig. 6. At the same time, some of the galaxies in the G3Cv04 group have been lost, as discussed at the end of Section 2.4.

In contrast, the two spatial substructure tests do not show major changes from G3Cv04 to G3Cv06 groups, with only a few showing more substructure than the original limits. The mirror symmetry gives a significant ($\geq$95 per cent) substructure result for groups 200043, 200099 and 200130. The angular symmetry test similarly highlights groups 200043 and 200099. The significant mirror symmetry result for 200130 is not surprising, given its intersection with the survey edge.

Comparing the substructure indices of the two non-detected groups with the others, we see that they have similar, moderate values of $\zeta_{\rm AD}$ (ranking fifth and sixth highest in the sample). For the spatial tests, the values for group 100053 are low, and typical of the rest of our sample, suggesting that it is a virialized system. In contrast, group 200099 shows some of the highest substructure in the sample (ranked first for $\zeta_\beta$ and second for $\zeta_{\rm AST}$). However, this may be related to the uncertainties in centring already noted,

**Table 5.** $M_{500}$ estimates (in units of $10^{13}\,M_{\odot}$, assuming $h_{70} = 1$) for our group sample.

| GroupID | $M_{L,\,\mathrm{GAMA}}$ | $M_{\sigma,\,\mathrm{GAMA}}$ | $M_N$ | $M_L$ | $M_\delta$ | $M_{\delta_L}$ | $M_\sigma$ | $M_{\mathrm{X\text{-}ray}}{}^a$ |
|---|---|---|---|---|---|---|---|---|
| 100053 | 5.91 | 6.46 | 3.84 | 6.40 | 2.50 | 2.46 | 1.06 | (−) |
| 200015 | 4.79 | 6.61 | 14.06 | 9.78 | 24.8 | 28.1 | 6.49 | $(3.16 \pm 0.83)$ |
| 200017 | 4.01 | 7.71 | 2.90 | 3.95 | 6.44 | 5.83 | 5.07 | $(4.74 \pm 2.33)$ |
| 200043 | 5.25 | 8.06 | 5.97 | 11.9 | 7.67 | 10.9 | 5.24 | $(2.77 \pm 1.47)$ |
| 200054 | 4.61 | 8.48 | 6.91 | 9.34 | 6.27 | 7.83 | 6.00 | $(16.2 \pm 7.53)$ |
| 200099 | 4.73 | 3.32 | 1.83 | 3.32 | 0.90 | 0.91 | 1.44 | (−) |
| 200115 | 2.62 | 4.50 | 0.45 | 0.54 | 2.40 | 1.55 | 1.63 | $(1.20 \pm 0.12)$ |
| 200130 | 7.22 | 13.1 | 4.17 | 7.15 | 8.05 | 3.91 | 9.89 | $(7.66 \pm 0.15)$ |
| 300008 | 3.60 | 8.88 | 2.89 | 3.98 | 6.43 | 4.22 | 4.22 | $(6.80 \pm 1.83)$ |
| 300067 | 2.63 | 3.03 | 1.21 | 1.00 | 1.27 | 0.95 | 1.68 | $(2.44 \pm 0.44)$ |

[a]For comparison, X-ray $M_{500}$ as reported in Table 2.

since 200099 has no obvious bright central galaxy. Recalculating substructure around a simple centre-of-light centroid, without iterating, we observe considerably less projected substructure, with $\zeta_\beta = 1.47\,(p = 0.94)$ and $\zeta_{\mathrm{AST}} = 1.42\,(p = 0.81)$. Whilst the lack of a dominant central galaxy could result from incomplete virialization of the group, we note that if it is a high-entropy group, then gas will be inhibited from cooling on to any central galaxy and fuelling growth through late star formation.

On the basis of substructure, we therefore conclude that we have no strong evidence that the groups 100053 and 200099 are not real, collapsed structures. This suggests that the observed high-entropy limits provide genuine indicators of the entropy of the gas in these systems.

### 5.3 Mass estimation quality

The ability to estimate masses is important for this work. It was the basis for the predicted X-ray fluxes that were used in selecting the sample for *Chandra* observation and is also used in the calculation of the group entropies. We have used the X-ray temperature to derive our mass estimates wherever possible, as described in Section 3.1, and as discussed in Section 4.1, we believe that our predicted temperatures, and therefore mass estimates, are, in general, unbiased, though highly scattered.

Nonetheless, it is of considerable interest to compare the results from different mass estimation techniques applied to our sample. A variety of mass estimates can be derived from analysis of the group galaxies using their dynamics, optical luminosity or spatial distribution. For groups that are simple, relaxed and virialized, and have typical star formation efficiency, we would expect to obtain good agreement between these different optical mass estimates. So, major differences between results from the different estimators may indicate groups that are unrelaxed or atypical. It is therefore highly relevant to examine whether this is the case for our two X-ray undetected groups.

The optical mass estimators we employ are mostly taken from the study of Pearson et al. (2015), and we therefore reselect the member galaxies for each of our groups using the method employed by these authors. Galaxies are extracted from a cylindrical volume with a projected radius of 1 Mpc and a velocity depth $\pm 3\sigma$ along the line of sight centred on the X-ray centroid where possible, where the velocity dispersion $\sigma$ is derived using the gapper estimator of Beers, Flynn & Gebhardt (1990). We refer to this galaxy sample as the volumetric group sample, in contrast to the GAMA FoF sample defined by Robotham et al. (2011). Using the volumetric sample, we construct a series of mass estimates based on (i) the observed group richness, (ii) luminosity (both extrapolated from the $m_r = 19.8$ mag flux limit to a standard limiting absolute magnitude $M_r = -16.5$ mag assuming a cluster luminosity function derived from the SDSS (Popesso et al. 2005), (iii) galaxy, (iv) luminosity overdensity (from fits to an NFW radial density profile (Navarro et al. 1996)), and (v) a dynamical mass estimator $\propto \sigma^{3\alpha}$. These mass estimates, labelled $M_N, M_L, M_\delta, M_{\delta_L}$ and $M_\sigma$, respectively, are based on mass–proxy relations that have been calibrated against $M_{500}$ from a sample of X-ray-selected groups, as described in Pearson et al. (2015).

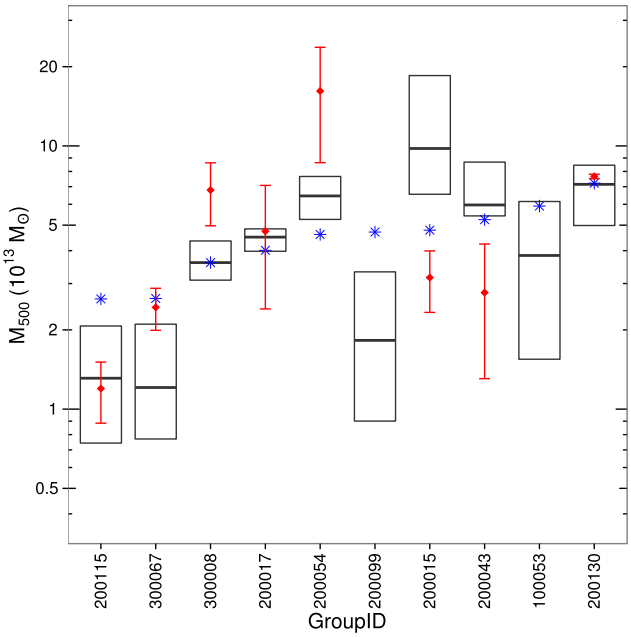


**Figure 7.** Distribution of predicted group $M_{500}$ ordered by the GAMA luminosity-predicted mass. Included in the boxplot are all mass estimates from Table 5 with the exception of X-ray-based mass estimates. The blue stars are the predicted masses used for the X-ray feasibility (derived from the GAMA luminosity), and the red diamonds are the $M$–$T$-based masses of Table 2. The boxes represent the median and 25th–75th quartiles of mass estimates.

In addition to these five galaxy-based mass estimators, we also include masses derived from GAMA FoF total light ($M_{L,\,\mathrm{GAMA}}$; see Section 2) and GAMA group masses derived from the FoF group velocity dispersion ($M_{\sigma,\,\mathrm{GAMA}}$; Robotham et al. 2011), calibrated on the GAMA mock data and applied to the G3Cv06 GAMA catalogue.

In Table 5 and Fig. 7, we summarize these mass estimates, and compare them with the X-ray-derived masses for the eight detected

systems. The boxplot in Fig. 7 shows the spread of mass estimates according to their interquartile range (IQR) for each group. With only seven masses going into each boxplot, the statistics here are limited, so definitive conclusions are difficult to draw. None the less, a number of interesting points can be noted.

As seen in Fig. 7, of the eight groups with detected X-ray emission, we see four groups (200115, 300067, 200017 and 200130) for which the X-ray-derived masses are consistent (within $1\sigma$) with the IQR of mass estimates. In the other four cases, the X-ray mass lies within about a factor of 2 of the interquartile box – above it in two cases and below it in two others.

The masses ($M_{L,\,\mathrm{GAMA}}$) predicted from the GAMA group optical luminosity were used to estimate the expected X-ray properties when selecting our sample for observation with *Chandra*. Comparing these masses (blue stars in Fig. 7) with the X-ray masses for the eight detected systems, we note that only one group (200115) had its mass overpredicted by more than a factor of 2. Since our substructure screening was estimated (Section 2.3) to leave a 6 per cent chance for a given group to have its mass overestimated by a factor of 2 or more, a binomial calculation shows that there is a 34 per cent chance for a sample of 10 groups to contain one group whose predicted properties are significantly overestimated. So, we should not be too surprised to find one case in the sample. Note, however, that the X-ray-derived mass for this system is contained well within the IQR of the whole set of optical mass estimators for this group.

Comparing the size of the IQR for each group, we see that the two groups with no diffuse X-ray emission also have the broadest IQR of the sample. Examining individual mass estimates, we see that both the dynamical, $M_\sigma$, mass for these groups and the overdensity-based masses, $M_\delta$ and $M_{\delta_L}$, are low compared to masses estimated from a simple count of light or number. Since the overdensity masses are derived by fitting the radial profiles of the group galaxies, the low values of these estimates suggest that these groups may be characterized by small overdense cores located within larger collapsing structures. This interpretation is strengthened by the fact that a similar discrepancy is observed between the overdensity and richness mass estimates for group 300067. As already noted, this group shows little diffuse emission other than a concentrated halo of emission around the central bright galaxy.

## 6 CONCLUSIONS

This study has investigated the hot gas properties of a small sample of galaxy groups selected to have good galaxy membership data from the GAMA survey and to show little optical substructure. Using data from the *Chandra Observatory*, we detect hot intergalactic gas in 8 of our 10 groups, and estimate X-ray temperatures, luminosities and central gas entropies, searching for evidence of the existence of groups with the high gas entropies predicted by some pre-heating models. Two of our groups are high-entropy candidates, with $2\sigma$ lower limits on central gas entropy that lie at the upper edge of the $1\sigma$ range predicted by the OWLS AGN feedback model. All other groups have entropies lying within the range found in X-ray-selected group samples, but with a median value shifted towards higher entropy, consistent with the reduced X-ray luminosity and gas fractions observed within our sample.

We have examined the robustness of our entropy limits against uncertainties in temperature or core radius, and conclude that these are unlikely to reduce our high upper limits into the range seen in normal X-ray-bright systems.

Two different approaches have been applied to investigate the possibility that these two high-entropy candidates may, notwithstanding our substructure screening, be uncollapsed or unvirialized systems. A closer examination of the substructure statistics, using the deeper GAMA data that became available since our initial sample was selected, does not reveal any convincing evidence for the two undetected groups being uncollapsed or unvirialized. However, our second test, comparing the mass estimates for the sample derived from a basket of galaxy-based mass estimators, does produce evidence that the high-entropy candidates may be 'special'. These are the two groups from our sample that show the largest discrepancies between the different galaxy-based mass estimates. In both cases, masses derived from the galaxy overdensity profiles or the velocity dispersion are substantially lower than those derived from richness or total group *r*-band luminosity. One possible interpretation that we suggest is that these two groups are not strongly substructured or asymmetrical (hence the low values from the substructure statistics) but are not yet fully collapsed.

Whether this possibility could account for the lack of detectable diffuse X-ray emission in these groups without the need to invoke high-entropy gas is not clear. In the absence of strong pre-heating, a collapsed core can still generate significant X-ray emission, as is seen in the case of group 300067. A definitive answer to the question of whether groups 100053 and 200099 contain high-entropy gas requires deeper X-ray observations that are able to detect the hot gas. It should be noted that these two systems are among the three shortest *Chandra* exposure times in our study.

In addition to the possibility of high-entropy gas within two of our groups, it is clear that our optically selected sample deviates significantly from the properties of typical X-ray-selected groups. The raised gas entropies and lower X-ray luminosities and gas fractions seen in our sample highlight the importance of selection effects when studying the properties of gas within collapsed groups.

Future deep X-ray studies of a larger sample of groups selected from the more recent GAMA data releases should provide strong constraints on the true distribution gas properties in collapsed groups independent of X-ray selection effects. This distribution can then be used to discriminate between competing models for the cosmic feedback arising from AGNs and supernovae. In this context, this study should be viewed as a pathfinder.

## ACKNOWLEDGEMENTS

RJP acknowledges the support of an STFC Postgraduate Studentship. PN and RGB acknowledge the support of the Science and Technology Facilities Council (ST/L00075X/1 and ST/P000541/1). PN also acknowledges the support of the Royal Society through the award of a University Research Fellowship. AB acknowledges support from NSERC (Canada) through the Discovery Grant programme and from the Pauli Center for Theoretical Studies ETH UZH. He would also like to thank the University of Zurich's Institute for Computational Sciences, and especially the members of the Institute's Center for Theoretical Astrophysics and Cosmology, for their hospitality during his recent extended visit. IGM is supported by an STFC Advanced Fellowship. We would also like to thank Alastair Sanderson and Ewan O'Sullivan for their assistance when selecting our groups, and an anonymous referee for valuable comments on this paper.

GAMA is a joint European-Australasian project based around a spectroscopic campaign using the Anglo-Australian Telescope. The GAMA input catalogue is based on data taken from the Sloan Digital Sky Survey and the UKIRT Infrared Deep Sky Survey. Complementary imaging of the GAMA regions is being obtained by a number of independent survey programmes, including *GALEX* MIS,

VST KiDS, VISTA VIKING, *WISE*, *Herschel*-ATLAS, GMRT and ASKAP, providing UV to radio coverage. GAMA is funded by the STFC (UK), the ARC (Australia), the AAO and the participating institutions. The GAMA website is http://www.gama-survey.org/.

## REFERENCES

Anderson M. E., Gaspari M., White S. D. M., Wang W., Dai X., 2015, MNRAS, 449, 3806
Babul A., Balogh M. L., Lewis G. F., Poole G. B., 2002, MNRAS, 330, 329
Balogh M. L., Babul A., Patton D. R., 1999, MNRAS, 307, 463
Balogh M. L., Pearce F. R., Bower R. G., Kay S. T., 2001, MNRAS, 326, 1228
Balogh M. L., Mazzotta P., Bower R. G., Eke V., Bourdin H., Lu T., Theuns T., 2011, MNRAS, 412, 947
Beers T. C., Flynn K., Gebhardt K., 1990, AJ, 100, 32
Bower R. G., Benson A. J., Malbon R., Helly J. C., Frenk C. S., Baugh C. M., Cole S., Lacey C. G., 2006, MNRAS, 370, 645
Bryan G. L., 2000, ApJ, 544, L1
Cash W., 1979, ApJ, 228, 939
Cavagnolo K. W., Donahue M., Voit G. M., Sun M., 2008, ApJ, 683, L107
Cavagnolo K. W., Donahue M., Voit G. M., Sun M., 2009, ApJS, 182, 12
Cavaliere A., Fusco-Femiano R., 1976, A&A, 49, 137
D'Agostino R. B., Stephens M. A., 1986, Goodness-of-Fit-Techniques, Statistics: Textbooks and Monographs. CRC Press, New York, p. 126
Davé R., Oppenheimer B. D., Sivanandam S., 2008, MNRAS, 391, 110
Donahue M., Horner D. J., Cavagnolo K. W., Voit G. M., 2006, ApJ, 643, 730
Driver S. P. et al., 2011, MNRAS, 413, 971
Eke V. R. et al., 2004, MNRAS, 348, 866
Ettori S., 2000, MNRAS, 318, 1041
Evrard A. E., Henry J. P., 1991, ApJ, 383, 95
Fukazawa Y., Kawano N., Kawashima K., 2004, ApJ, 606, L109
Gonzalez A. H., Sivanandam S., Zabludoff A. I., Zaritsky D., 2013, ApJ, 778, 14
Grevesse N., Sauval A. J., 1998, Space Sci. Rev., 85, 161
Gross J., Ligges U., 2012, NORTEST: Tests for Normality. R package version 1.0-2. Available at: https://CRAN.R-project.org/package=nortest
Han J. et al., 2015, MNRAS, 446, 1356
Helsdon S. F., Ponman T. J., 2000, MNRAS, 315, 356
Hopkins A. M. et al., 2013, MNRAS, 430, 2047
Hudson D. S., Mittal R., Reiprich T. H., Nulsen P. E. J., Andernach H., Sarazin C. L., 2010, A&A, 513, A37
Humphrey P. J., Liu W., Buote D. A., 2009, ApJ, 693, 822
Jiang L., Helly J. C., Cole S., Frenk C. S., 2014, MNRAS, 440, 2115
Kaiser N., 1991, ApJ, 383, 104
Kalberla P. M. W., Burton W. B., Hartmann D., Arnal E. M., Bajaja E., Morras R., Pöppel W. G. L., 2005, A&A, 440, 775
Koutroumpa D., Lallement R., Kharchenko V., Dalgarno A., 2009, Space Sci. Rev., 143, 217
Kuntz K. D., Snowden S. L., 2008, A&A, 478, 575
Le Brun A. M. C., McCarthy I. G., Schaye J., Ponman T. J., 2014, MNRAS, 441, 1270
Lewis G. F., Babul A., Katz N., Quinn T., Hernquist L., Weinberg D. H., 2000, ApJ, 536, 623
Liang L., Durier F., Babul A., Davé R., Oppenheimer B. D., Katz N., Fardal M., Quinn T., 2016, MNRAS, 456, 4266
Liske J. et al., 2015, MNRAS, 452, 2087
Lloyd-Davies E. J., Ponman T. J., Cannon D. B., 2000, MNRAS, 315, 689
Loveday J. et al., 2012, MNRAS, 420, 1239
McCarthy I. G., Balogh M. L., Babul A., Poole G. B., Horner D. J., 2004, ApJ, 613, 811
McCarthy I. G., Babul A., Bower R. G., Balogh M. L., 2008, MNRAS, 386, 1309
McCarthy I. G. et al., 2010, MNRAS, 406, 822
McCarthy I. G., Schaye J., Bower R. G., Ponman T. J., Booth C. M., Dalla Vecchia C., Springel V., 2011, MNRAS, 412, 1965
McKee C. F., Cowie L. L., 1977, ApJ, 215, 213
Merson A. I. et al., 2013, MNRAS, 429, 556
Mohr J. J., Mathiesen B., Evrard A. E., 1999, ApJ, 517, 627
Navarro J. F., Frenk C. S., White S. D. M., 1996, ApJ, 462, 563
Osmond J. P. F., Ponman T. J., 2004, MNRAS, 350, 1511
Pascut A., Ponman T. J., 2015, MNRAS, 447, 3723
Pearson R. J., Ponman T. J., Norberg P., Robotham A. S. G., Farr W. M., 2015, MNRAS, 449, 3082
Pinkney J., Roettiger K., Burns J. O., Bird C. M., 1996, ApJS, 104, 1
Ponman T. J., Cannon D. B., Navarro J. F., 1999, Nature, 397, 135
Popesso P., Böhringer H., Romaniello M., Voges W., 2005, A&A, 433, 415
Popesso P., Biviano A., Böhringer H., Romaniello M., 2007, A&A, 464, 451
Pratt G. W., Croston J. H., Arnaud M., Böhringer H., 2009, A&A, 498, 361
R Development Core Team, 2009, R: A Language and Environment for Statistical Computing. R Foundation for Statistical Computing, Vienna
Rasmussen J., Ponman T. J., 2007, MNRAS, 380, 1554
Rasmussen J., Ponman T. J., Mulchaey J. S., Miles T. A., Raychaudhury S., 2006, MNRAS, 373, 653
Robotham A. S. G. et al., 2011, MNRAS, 1172
Sanderson A. J. R., O'Sullivan E., Ponman T. J., 2009, MNRAS, 395, 764
Sanderson A. J. R., O'Sullivan E., Ponman T. J., Gonzalez A. H., Sivanandam S., Zabludoff A. I., Zaritsky D., 2013, MNRAS, 429, 3288
Schaye J. et al., 2010, MNRAS, 402, 1536
Slack N. W., Ponman T. J., 2014, MNRAS, 439, 102
Springel V. et al., 2005, Nature, 435, 629
Sun M., Jones C., Forman W., Vikhlinin A., Donahue M., Voit M., 2007, ApJ, 657, 197
Sun M., Voit G. M., Donahue M., Jones C., Forman W., Vikhlinin A., 2009, ApJ, 693, 1142
Tankard-Evans T. A., 2015, The Role of Environment in Galaxy Formation. Durham theses, Durham University. Available at Durham E-Theses Online: http://etheses.dur.ac.uk/11345/
Thode H. C., 2002, Testing For Normality, Statistics: Textbooks and Monographs. CRC Press, New York, p. 104
Tozzi P., Norman C., 2001, ApJ, 546, 63
Vikhlinin A., Forman W., Jones C., 1999, ApJ, 525, 47
Vikhlinin A., Markevitch M., Murray S. S., Jones C., Forman W., Van Speybroeck L., 2005, ApJ, 628, 655
Vikhlinin A., Kravtsov A., Forman W., Jones C., Markevitch M., Murray S. S., Van Speybroeck L., 2006, ApJ, 640, 691
Viola M. et al., 2015, MNRAS, 452, 3529
Voit G. M., 2005, Rev. Mod. Phys., 77, 207
Voit G. M., Bryan G. L., 2001, Nature, 414, 425
Voit G. M., Kay S. T., Bryan G. L., 2005, MNRAS, 364, 909
West M. J., Oemler A. Jr, Dekel A., 1988, ApJ, 327, 1
Wu K. K. S., Fabian A. C., Nulsen P. E. J., 2000, MNRAS, 318, 889

This paper has been typeset from a TEX/LATEX file prepared by the author.